Preparation of Pt/γ-Al2O3 catalyst coating in microreactors for catalytic methane combustion

He, Li; Fan, Yilin; Luo, Lingai; Bellettre, Jerome; Yue, Jun

Published in:
Chemical Engineering Journal

DOI:
10.1016/j.cej.2019.122424

Publication date:
2020

Chemical Engineering Journal 380 (2020) 122424

Contents lists available at ScienceDirect

Chemical Engineering Journal

journal homepage: www.elsevier.com/locate/cej

Preparation of Pt/γ-Al_2O_3 catalyst coating in microreactors for catalytic methane combustion

Li He[a,b], Yilin Fan[b], Lingai Luo[b], Jérôme Bellettre[b,*], Jun Yue[a,*]

[a] Department of Chemical Engineering, Engineering and Technology Institute Groningen, University of Groningen, 9747 AG Groningen, The Netherlands
[b] Université de Nantes, CNRS, Laboratoire de thermique et énergie de Nantes, LTeN, UMR 6607, F-44000 Nantes, France

HIGHLIGHTS

- γ-Al_2O_3 washcoated on FeCrAlloy substrates exhibited excellent adhesion.
- γ-Al_2O_3 particle size and pH are important factors affecting the slurry stability.
- Polyvinyl alcohol as the binder effectively enhanced the washcoat adhesion.
- Pt/γ-Al_2O_3 coated in microreactors catalyzed methane combustion efficiently.
- Temperature and oxygen-to-methane ratio greatly affected the methane conversion.

ARTICLE INFO

Keywords:
Microreactor
γ-Alumina
Catalytic coating
Catalytic combustion
Methane
Temperature distribution

ABSTRACT

A catalyst preparation method, consisting of slurry washcoating with γ-Al_2O_3 followed by impregnating platinum on the microreactor walls, has been investigated. The effect of various factors in the preparation procedures on the adhesion of the washcoated γ-Al_2O_3 was studied, including the slurry property (i.e., the binder type, concentration and molecular weight, γ-Al_2O_3 concentration and particle size, pH), and the (micro)reactor substrate and channel shape. The results show that the adhesion of γ-Al_2O_3 washcoat strongly depended on the slurry rheological characteristics. A good adhesion on FeCrAlloy substrates was obtained using the slurry with polyvinyl alcohol as the binder (typical concentration at 3–5 wt% and molecular weight of 57,000–186,000), 20 wt% γ-Al_2O_3 (particle size being around 3 μm) and pH = 3.5. FeCrAlloy as the substrate exhibited an excellent coating adhesion in rectangular or round channels, primarily due to the formation of alumina film over the surface during thermal pretreatment. The aluminum-free stainless steel as the substrate only showed a good adhesion in a round channel. Well-adhered Pt/γ-Al_2O_3 catalysts were then applied in a microreactor comprising parallelized microchannels made of FeCrAlloy under the optimized coating procedures, and investigated in terms of its performance in the catalytic methane combustion. It is shown that the reaction temperature has a greater influence on the methane conversion than the flow rate, and a favorable coverage of methane and oxygen on the catalyst surface is essential to obtain a good catalytic performance. These reaction results are in line with the temperature behavior measured along the microreactor.

1. Introduction

Microreactors, with characteristic channel dimensions on the order of ca. 1 mm or below, have shown great potentials in intensifying reaction processes in comparison to conventional reactors (e.g. fixed-bed reactors for solid-catalyzed gas phase and multiphase reactions) [1–3]. The specific surface area of microreactors could reach 10,000 to 50,000 $m^2 m^{-3}$ [4,5], compared to around 100 $m^2 m^{-3}$ for traditional reactors, thereby leading to substantially enhanced mass and heat transfer rates [6,7]. The improved mass transfer can lead to enhanced reaction rates (e.g., in the presence of multiphase fluids or solid catalysts). The heat transfer enhancement avoids the presence of temperature hot spots due to the local accumulation of reaction heat in the microreactor, a feature especially favorable for handling strongly exothermic reactions or coupled exothermic and endothermic catalytic reactions [8]. Moreover, the modular, flexible and compact microreactor design allows an easy upscaling from the laboratory to the industrial scale aiming at mass production [4]. One challenge is how to

* Corresponding authors.
E-mail addresses: jerome.bellettre@univ-nantes.fr (J. Bellettre), yue.jun@rug.nl (J. Yue).

https://doi.org/10.1016/j.cej.2019.122424
Received 7 May 2019; Received in revised form 2 August 2019; Accepted 4 August 2019
Available online 06 August 2019

Nomenclature

d_C	Inner diameter of the channel, m
$F_{CH_4,i}$	Inlet molar flow rate of CH_4, mol s^{-1}
$F_{CH_4,o}$	Outlet molar flow rate of CH_4, mol s^{-1}
$F_{CO_x,o}$	Outlet molar flow rate of CO or CO_2, mol s^{-1}
ΔH_R	Heat of reaction for methane combustion, kJ mol^{-1}
L	Length of the channel, m
L^*	Normalized length of the channel (Eq. (3))
Q_{tot}	Total volumetric flow rate, m^3 s^{-1}
S_{CO_x}	Selectivity of CO or CO_2 (Eq. (2))
ΔT_{ad}	Adiabatic temperature rise, °C or K
V_{tot}	Total volume of channels for reaction in a multi-channel microreactor, m^3
X_{CH_4}	CH_4 conversion (Eq. (1))

Greek symbols

τ	Residence time, s (Eq. (4))
Φ	Inlet molar ratio of oxygen to methane

Abbreviation

BET	Brunauer-Emmett-Teller
GC	Gas chromatography
2-HEC	2-Hydroxyethyl cellulose
MW	Molecular weight
PEG	Polyethylene glycol
PVA	Polyvinyl alcohol
SEM	Scanning electron microscopy
TGA	Thermogravimetric analysis
Tylose	Methyl 2-hydroxyethyl cellulose

deliver reaction fluids, as well as heat transfer fluids (if present), uniformly across a multitude of microchannels in order to ensure that the optimal microreactor performance is not lost during the numbering-up process (i.e., a replication of basic microchannel units) [9–11].

Solid catalysts (e.g., noble metal-based) can be incorporated into microreactors as wall coatings, and γ-Al_2O_3 represents one of the most common catalyst supports in use. Thus, a successful application of microreactors for solid-catalyzed catalytic reactions strongly depends on the formation of a well-adhered and uniform catalyst layer on the microreactor substrate [12,13]. Based on the properties of the catalyst and substrate surface, various methods have been used to deposit catalysts onto the microreactor wall, as summarized in some reviews [12,14,15]. Different coating methods and the corresponding preparation procedures have been investigated, including suspension [16–18], sol-gel deposition [19,20], electrophoretic deposition [21,22], chemical vapor deposition [23,24], physical vapor deposition [25,26], etc. The suspension technique (or slurry washcoating) is one of the most commonly used methods for depositing catalysts in microreactors, which typically consists of the following steps: microreactor surface pretreatment, slurry preparation and deposition, impregnation of the catalytically active component (e.g., noble metal), heat treatment (e.g., drying and calcination). Sometimes, a primer coating is used before the slurry deposition to further enhance the coating adhesion. Alternatively, the catalytically active component can be mixed with the prepared slurry prior to the coating step, allowing to attach the entire catalyst onto the microreactor wall in one step. It has been reported that the slurry properties (e.g., the binder nature, viscosity, pH and particle size) could greatly influence the rheological properties of the washcoated layer as well as its adhesion [27]. A brief literature survey of key factors in these steps is presented below, including the substrate pretreatment, nature of binder, pH and particle sizes used in the slurry for washcoating, and primer coating.

The thermal pretreatment of the (microreactor) substrate is the most commonly used method to increase the substrate surface roughness. In the case of Al-containing substrates, such pretreatment also causes the migration of aluminum species over the substrate surface to form a thin film, effectively enhancing the adhesion between the coating layer and substrate. For instance, the thermal pretreatment of FeCrAlloy material could be conducted in a range of 800 to 1000 °C for 5 to 10 h [28–30]. It has been reported that alumina crystals appeared at about 700 °C. When the calcination temperature was increased to 900 °C, the needle-like α-Al_2O_3 was substantially formed and tended to cover the whole surface. This is beneficial for anchoring the deposited washcoated layer. The rapid growth of α-Al_2O_3 grains and the agglomeration occurred at 1000 °C, forming the globular morphology. Other pretreatment methods such as the anodic oxidation on aluminum or aluminum alloy plates [31,32] and the chemical pretreatment on substrates made of aluminum, FeCrAlloy or stainless steel [33,34] were also reported.

The suspension method was characterized typically by adding the binder into a slurry (e.g., of γ-Al_2O_3), in order to finally form a smooth and well-adhered layer onto the walls of microreactors [35,36]. Binders are generally divided into two categories: organic binder (e.g., polymers) and inorganic binder (e.g., boehmite and colloidal alumina). The effect of different binders on the coating adhesion was investigated by Germani et al. [37]. A compromise between the shrinking behavior and particle packing of the coating could be reached using methyl 2-hydroxyethyl cellulose (Tylose) as the binder which has a better thickening effect compared to polyvinyl alcohol (PVA). Besides the binder structure, its molecular weight and concentration may also have a noticeable effect on the slurry viscosity and subsequently the prepared coating adhesion. An excessive addition of organic binders could result in cracks during calcination due to the polymer thermal decomposition [37]. Details on the binder characterization may be found elsewhere [38–40].

For washcoating of γ-Al_2O_3, the slurry stability also depends on whether γ-Al_2O_3 particles are well dispersed in the suspension. The viscosity and stability of the slurry greatly increase with the increasing pH value. This is because the net surface charge of particles is changed by adjusting the pH [41]. The initial particle size of γ-Al_2O_3 is also a key factor that affects the adhesion strength. Particle sizes of 2–5 μm were reported to be a suitable range to obtain a stable slurry [27,39,42], because a smaller particle size improved the affinity and interlocking between particles in the coating.

Apart from directly applying slurry onto the microreactor wall, an intermediate layer of primer coating can be deposited in a previous step, acting as a link to enhance the adhesion between the substrate and the slurry deposition. Moreover, the difference in thermal expansion coefficients between the washcoated layer and the substrate could be decreased to some extent by applying primer coating in between. Various primer compositions have been investigated and optimized [17,43]. In order to further improve the coating adhesion on Al-free substrates like stainless steel, the substrate could be treated by the pack aluminisation technique before the primer coating step [44,45]. A thin alumina layer is expected to form on stainless steel by the diffusion of metal atoms over the surface.

Microreactors with wall-coated catalysts are promising for carrying out the catalytic combustion of methane efficiently. Compared with the conventional flame combustion, the catalytic methane combustion has been performed towards achieving a lower light-off or working temperature, less exhaust emission and more stable combustion [46]. Catalyst development, reactor design and operational conditions should be thus well addressed for obtaining an optimal process performance. Noble metal-based catalysts with high specific surface areas were reported to have a better catalytic performance than perovskites or

hexaaluminate catalysts in the catalytic methane combustion, with lower activation energy, less pollutant and lower light-off temperature allowing more stable combustion [47,48]. Pd, Pt, Rh and Au as the active component have been widely studied [49]. Among them, Pd and Pt-based catalysts were reported as the most active one by far. The base/acid properties of the support affect the catalytic activity by interacting with the oxidized/metallized state of noble metals. It was reported that the decreased acidity strength of Al_2O_3 support (e.g., with Pd as the active component) could enhance the catalytic performance of methane combustion [50]. Pt/Al_2O_3 catalyst has also shown to be more active when the O_2/CH_4 molar ratio was varied from the oxygen-rich to methane-rich conditions [48]. So far, many studies have been performed to characterize the performance of catalytic methane combustion, but mostly in conventional fixed-bed reactors [51,52] or monolithic reactors [53,54]. Fewer studies were devoted to wall-coated microreactors that are promising owing to their enhanced mass and heat transfer rates, leading to a better process control in terms of high reaction rates and suppressing temperature excursion [55–57]. Especially, plate-type multi-channel microreactors, with appropriate catalyst coatings, seem very attractive for use in the catalytic methane combustion, allowing a modular and compact coupling with heat transfer (for the utilization of the combustion reaction heat) or with an endothermic reaction (e.g., steam reforming), which becomes a research hotspot in the recent decade for the foreseeable industry benefits [58–60].

From the above literature survey, one may find that the research on how to obtain a good adhesion and dispersion of the catalytic layer onto the walls of microreactors is still needed, especially when it comes to γ-Al_2O_3 supported noble metal catalysts for use in the catalytic methane combustion. Thus, the main objective of this study is to investigate and characterize the slurry washcoating method of γ-Al_2O_3 onto microreactor walls, so as to ensure the formation of a stable, homogeneous and well-adhered catalyst layer. The effect of various factors in the preparation procedures was systematically studied, including the slurry property (i.e., the binder nature and its concentration and molecular weight, the pH value, the γ-Al_2O_3 content and particle size), and the (micro)reactor substrate material and channel shape. Then, washcoating of γ-Al_2O_3 under the optimized preparation conditions, followed by the impregnation of platinum, was used to prepare Pt/γ-Al_2O_3 catalyst on the walls of a laboratory-scale multi-channel microreactor made of FeCrAlloy. The microreactor performance was tested in the catalytic methane combustion, where the influence of operating conditions and the temperature distribution along the microreactor have been particularly addressed.

2. Experimental

2.1. Materials

γ-Al_2O_3 (3 μm, 99.97% on metals basis), PVA (98–99% hydrolyzed), acetic acid, tetraammineplatinum (II) nitrate ($Pt(NH_3)_4(NO_3)_2$, 99.99% on metals basis) were purchased from Alfa Aesar. Tylose MH300 (methyl 2-hydroxyethyl cellulose, molecular weight (MW) of 95,000), 2-HEC (2-hydroxyethyl cellulose, MW of 90,000), PEG (polyethylene glycol, MW of 20,000) were obtained from Sigma-Aldrich. γ-Al_2O_3 with other particle sizes (20 nm − 180 μm) were also studied and obtained from Sigma-Aldrich. Boehmite (AlO(OH)) and dispersal P2 were obtained from Sasol.

The multi-channel platelets used for the coating adhesion test were made of FeCrAlloy (Kanthal A-1, 22% Cr, 5.8% Al and Fe for balance) and 316 L stainless steel, having an overall dimension of 50 mm (length) × 22 mm (width) × 3 mm (height). 10 parallel microchannels of rectangular shape with a dimension of 50 mm × 1.5 mm × 1 mm were machined on each platelet. Round capillaries made of FeCrAlloy and 316 L stainless steel having a dimension of 10 mm (outer diameter; o.d.) × 8 mm (inner diameter; i.d.) × 100 mm (length) and square capillaries made of 316 L stainless steel with a dimension of 8 mm (width) × 8 mm (height) × 100 mm (length) were used for coating adhesion test as well.

The catalytic methane combustion was performed in plate-type multi-channel microreactors. The microreactor basically consisted of two multi-channel platelets (made of FeCrAlloy or 316 L stainless steel) back-to-back and enclosed by two additional blind stainless steel plates (350 mm × 80 mm × 5 mm). Each platelet (317.5 mm × 50 mm × 3 mm) has 16 parallelized straight channels of 275 mm × 1.5 mm × 1 mm, the total number of machined microchannels in the microreactor being 32 (Fig. 1). Each platelet has an inlet fluid distributor and an outlet fluid collector, having a bifurcated tree-like geometry (Fig. 1) that guarantees a uniform fluid flow distribution across parallel microchannels [61,62]. Only the two sides and bottom of the rectangular microchannel on the platelets

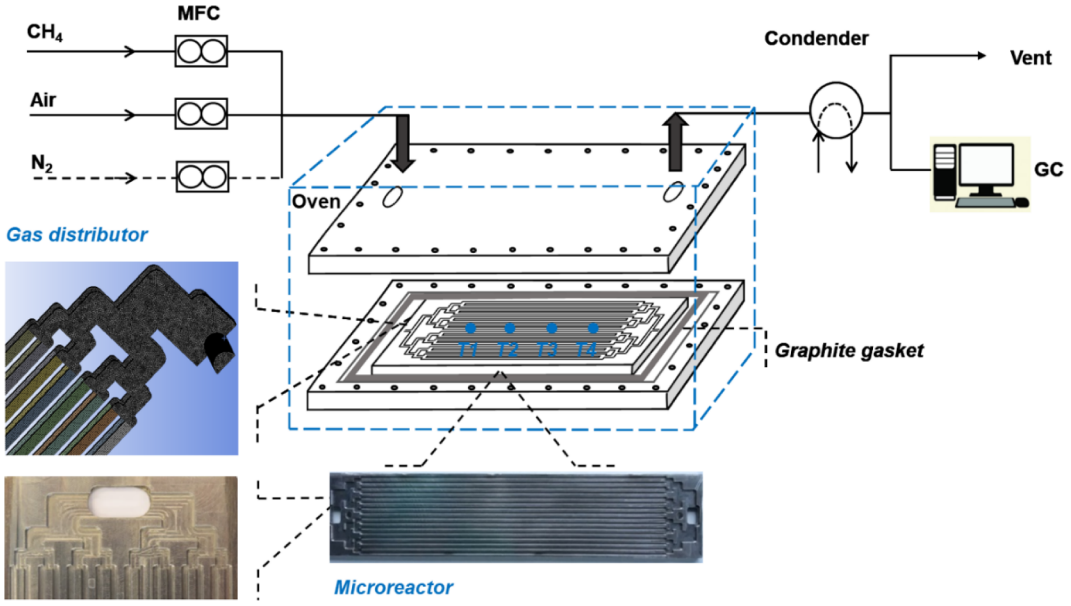

Fig. 1. Scheme of the catalytic methane combustion in the multi-channel microreactor coated with Pt/γ-Al_2O_3 catalyst. Thermocouples were placed at an axial distance to the beginning of the microchannels (T1: 55 mm, T2: 110 mm, T3: 165 mm, T4: 220 mm).

were coated with Pt/γ-Al_2O_3 catalyst, the fluid distributor and collector being not coated.

2.2. Catalyst preparation

2.2.1. Pretreatment

The platelets and capillaries made of FeCrAlloy were first immersed with acetone for 30 min in the ultrasonic bath at 45 °C, in order to remove oil, grease and other dirt [63]. Thermal pretreatment was subsequently performed at 900 °C (ramp from room temperature: 20 °C min^{-1}; 10 h at final temperature), to generate a thin alumina layer over the substrate surface which could be a strong bonding between the coating layer and the substrate [28,43]. In the case of platelets and capillaries made of 316 L stainless steel, sandblasting was first applied before the calcination pretreatment to remove the anti-corrosion layer on the surface as well as to increase its roughness.

2.2.2. Washcoating procedures

The γ-Al_2O_3 slurry was prepared by mixing γ-Al_2O_3 powders, binder and acetic acid [18]. Various binders (including Tylose, PVA, 2-HEC, PEG or boehmite) with different concentrations and/or molecular weights have been added in the slurry. γ-Al_2O_3 concentration was varied from 10 to 40 wt%, with its initial particle size ranging from 0.02 to 180 μm. pH of the slurry was changed from 1.5 (by adding acetic acid) to 9.35 (by adding NH_4OH). The slurry was then heated up to 65 °C for 2 h under 300 rpm stirring and stored at room temperature for at least 2 weeks to remove the inside bubbles before use.

Thus prepared slurry as the catalyst support precursor was first deposited on the walls of the parallelized microchannels on the microreactor platelets (made of FeCrAlloy and stainless steel) using syringe injection. The excessive suspension outside the microchannel was immediately removed with a razor blade. The platelets were then dried at room temperature overnight for at least 8 h, dehydrated at 120 °C for 8 h and finally calcined at 600 °C (ramp from room temperature: 2 °C min^{-1}; 2 h at final temperature). Multiple layers of coatings were obtained by repeating the same washcoating procedure as described above. A similar washcoating procedure was applied for coating inside circular or square capillaries, except that after the slurry washcoating, a rotary motor held one end of the capillary with a fixed rotation speed (ca. 30 rpm), keeping it at room temperature overnight. The same drying and calcination processes were then followed (see Appendix A for more details about washcoating in such capillaries).

The primer coating was only tested on the 316 L stainless steel multi-channel platelet (with 10 parallel microchannels; dimensions shown in Section 2.1) before coating the slurry. The alumina sol–gel composed of 10 wt% dispersal P2, 3% PVA (MW of 146,000–186,000) and 1% HNO_3 was coated on the platelet by using syringe injection. Subsequently, the substrate was dried at room temperature overnight (for at least 8 h) and then dehydrated at 120 °C for 8 h. Then, calcination at 600 °C for 2 h took place before applying the same slurry deposition procedure as describe above.

2.2.3. Impregnation of catalytically active component

The incipient wetness impregnation was performed by immersing the coated multi-channel platelet in a $Pt(NH_3)_4(NO_3)_2$ solution with a certain concentration. The impregnated coating was dried at room temperature overnight for at least 8 h, and then calcined at 450 °C (ramp from room temperature: 2 °C min^{-1}; 2 h at final temperature). The nominal Pt loading over the catalyst is about 3.8 wt% for the FeCrAlloy platelet, and about 3.5 wt% for the 316 L stainless steel platelet.

2.3. Washcoat adhesion test

The adhesion test of the prepared γ-Al_2O_3 washcoat was firstly performed by immersing the coated substrate in a glass beaker (containing acetone) that was placed in the ultrasonic bath (PCE-UC 20) for typically 3 h, the frequency of ultrasonic bath being 40 kHz. The weight loss of the substrate (i.e., multi-channel platelets or capillaries) was calculated based on its weight difference before and after the ultrasonic treatment combined with drying at room temperature. Another method used to test the adhesion is the thermal shock test, by rapidly heating the coated substrate to 800 °C (ramp: 20 °C min^{-1}) and cooling it down quickly to room temperature in the air, and repeating the cycle for 5 runs. The weight loss (i.e., the weight difference before and after the thermal shock test) was also measured.

2.4. Catalytic methane combustion in microreactors

Two mass flow controllers (MFC, Brooks SLA5850) were used to adjust the flow rates of methane and the synthetic air for the experiment (Fig. 1). The total gas flow rate was typically adjusted from 110 to 880 mL min^{-1} (based on ca. 20 °C and 1 atm). Methane-air mixture (concentration of methane at 2–10 vol%) first passed the inlet stainless steel tube (i.d.: 3.7 mm, o.d.: 6 mm). A part of this tube (15 cm in length) was kept inside an oven to preheat the mixture gas to the required reaction temperature. Then, the gas mixture was introduced into the multi-channel microreactor (i.e., with parallel microchannels on the platelet made of FeCrAlloy or 316 L stainless steel) placed in the oven. It has to be mentioned that the microreactor was first heated up (ramp: 10 °C min^{-1}) to the targeted reaction temperature under the nitrogen atmosphere to avoid any reaction occurrence during this startup process, and then the gas was switched to the methane-air mixture for the reaction to start. The reaction temperature tested ranged from 300 to 450 °C, and refers to the measured oven temperature by a thermocouple located in its right corner (Fig. 1). Four thermocouples (T1-T4) were placed on the top surface of the microreactor at different axial positions (i.e., at 20%, 40%, 60% and 80% of the microchannel length from the inlet), touching the top of the middle microchannel (Fig. 1). The product gas first flew through a condenser at the outlet of the microreactor to remove water, and was collected and analyzed using a gas chromatography (GC).

2.5. Analytical procedure

Gas product was collected by a Tedlar sample bag (SKC 3 L, 9.5 × 10 in.) with a single polypropylene septum fitting, and then analyzed by GC (Hewlett-Packard 5890 Series II) equipped with a thermal conductivity detector. A Porablot Q Al_2O_3/Na_2SO_4 column (length: 50 m; i.d.: 0.5 mm) and a CP-Molsieve 5 Å column (length: 25 m; i.d.: 0.53 mm) were used. The concentrations of the reference gas used were 20.7% CH_4, 17.9% CO_2, 2.99% CO, 1.5% C_2H_6, 1.49% C_3H_8, 5088 ppm C_2H_4, 5122 ppm C_3H_6 and H_2 for the rest. The GC oven temperature was heated from 40 °C up to 90 °C (ramp: 20 °C min^{-1}) and maintained for 7.5 min. The detector temperature was kept at 200 °C.

The rheological characteristics of slurries used for washcoating were evaluated by a rheometer (HAAKE Mars III, Thermo Scientific). The diameter of cone-and-plate geometry is 60 mm, the angle 2 °C. The slurry viscosity was measured based on a shear rate in a range of 0.05–1500 s^{-1} at 20 °C.

Zeta potential of the slurry as a function of pH was measured on a ZetaPALS instrument (Brookhaven) by the use of an electrophoretic technique. The mobility of charged particles can be determined via this technique by the phase analysis light scattering (PALS).

Thermogravimetric analysis (TGA) of the γ-Al_2O_3 slurry was performed on a PerkinElmer TGA 4000 thermogravimetric analyzer. The slurry was heated up in nitrogen from 30 °C to 1000 °C (at 10 °C min^{-1}). Data were recorded by Pyris thermal analysis software.

Scanning electron microscopy (SEM) was performed on an XL30 ESEM (Philips) operating at 20 keV, to characterize the smoothness and thickness of the washcoated γ-Al_2O_3 layer on the microchannel. The specific surface area of the washcoated γ-Al_2O_3 or Pt/γ-Al_2O_3 catalyst

was measured using a Micromeritics ASAP 2420 apparatus by nitrogen physisorption at −196 °C. The coating was scraped from the substrate and ground to a particle size below 25 μm. The samples were firstly degassed in the vacuum at 200 °C for 8 h before nitrogen adsorption. The surface area and pore size were evaluated using the Brunauer-Emmett-Teller (BET) method, and the micropore area was quantified by the t-plot method.

Transmission electron microscopy (TEM) analysis of the coated Pt/γ-Al_2O_3 catalyst was performed using an electron microscope CM12 (Philips) at 120 keV. The catalyst was scraped from the substrate and ground to a particle size below 25 μm, and prepared by ultrasonication in acetone.

2.6. Definitions

The loading (unit: g m^{-2}) of γ-Al_2O_3 or Pt/γ-Al_2O_3 deposited on a multi-channel platelet is calculated as its weight gained on the substrate (i.e., after calcination) divided by the microchannel surface area subject to coating.

The CH_4 conversion (X_{CH_4}) and CO_2 (CO) selectivity (S_{CO_x}) are calculated based on Eqs. (1) and (2), respectively.

$$X_{CH_4} = \frac{F_{CH_4,i} - F_{CH_4,o}}{F_{CH_4,i}} \times 100\% \quad (1)$$

$$S_{CO_x} = \frac{F_{CO_x,o}}{F_{CH_4,i} - F_{CH_4,o}} \times 100\% \quad (2)$$

Here F means the molar flow rate. The subscripts i and o indicate the microreactor inlet and outlet, respectively.

The normalized length (L^*) is used to infer the thermocouple location in the multi-channel microreactor (Fig. 1). It is defined as the distance from the thermal couple to the beginning of the parallel microchannel in which it was inserted (x) divided by the entire length of the microchannel (L).

$$L^* = \frac{x}{L} \quad (3)$$

The residence time (τ) in the multi-channel microreactor is defined as the total volume of the parallel microchannels (V_{tot}) divided by the total volumetric flow rate of the gas entering the microreactor (Q_{tot}).

$$\tau = \frac{V_{tot}}{Q_{tot}} \quad (4)$$

3. Results and discussion

3.1. Effect of preparation procedures on the washcoat adhesion

Many factors can have an important effect on the adhesion and thickness of the washcoated γ-Al_2O_3 layer over the metal substrate surface, including among others the binder characteristics and the slurry properties. The influence of these key factors is discussed in the following sub-sections.

3.1.1. Effect of binder

The multi-channel FeCrAlloy platelets were initially coated with slurries containing different binders. The slurry composition is listed in Table 1. Fig. 2 shows that the results from the ultrasonic test are in good agreement with the thermal shock test results in Table 1, with regard to the influence of binder addition on the washcoat adhesion strength: PVA (5 wt%) ≈ Tylose (1.6 wt%) > PVA (5 wt%) + boehmite (1 wt%) > 2-HEC (1.6 wt%) > PEG (15 wt%) > without binder. Typically, well-adhered and stable washcoated layers were obtained on the parallel microchannels of the platelets by employing PVA or Tylose as the binder. No weight loss of the washcoat was observed for the case with PVA in the ultrasonic test after 3 h and only 1.2 wt% weight loss for the case with Tylose, with no weight loss found in the thermal shock test. A higher weight loss of 8 wt% according to the ultrasonic test was caused by adding boehmite with PVA in the slurry. In this case, a strong shrinkage behavior was observed during drying overnight at room temperature, which resulted in a higher washcoat detachment. PEG or 2-HEC as the binder presented a much higher detachment from the microchannel wall, finally resulting in 78.9 wt% or 69.5 wt% weight losses in the ultrasonic test, respectively (Fig. 2). Fig. 2 also shows that the weight loss curves with all binders tested reach a plateau after 1 or 2 h ultrasonic treatment, indicating that at least part of (if not all) the washcoated layer was strongly anchored to the microchannel wall in all cases.

The slurry viscosity can be adjusted by changing the binder and its concentration (Fig. 3). The slurry viscosity exponentially rises with the increasing binder percentage, especially for PVA. It was reported that the hydroxyl methyl cellulose could act as an associative function group in the acid environment [64]. The high amount of hydroxyl group is able to aid the adhesion and the bond between particles [65]. Thus, binders (like PVA and Tylose) with a large amount of hydroxyl group on their surface could form a stronger bridge between particles, enhancing effectively the adhesion. However, the hydroxyl group of PEG is located only at the end of polymer chains, which is not enough to form a firm bonding with alumina, thus causing a poor washcoat adhesion as shown in Table 1 and Fig. 2 [5,66].

As shown in Fig. 3, Tylose and 2-HEC carrying methyl and hydroxyethyl groups have a more significant effect on the slurry viscosity increase even at a lower concentration than the case with PVA. As for PEG, in order to obtain a similar viscosity, a factor of 15 in terms of concentration is required than for Tylose or 2-HEC. The slurry viscosity is not always directly related to the washcoat adhesion strength. However, the viscosity reflects the interaction of the entangled long-chain binder with γ-Al_2O_3. Hence, an enhanced adhesion is expected to be obtained by using the slurry with a suitable viscosity.

During the drying process of the washcoated layer, the binder particles were attached to the surface of alumina and strong bridges could thus be formed. Different types of hydrogen bridges could be formed in terms of different surface groups of γ-Al_2O_3 [67]. On one hand, PVA carrying the hydroxyl group (–OH) may serve as the anchoring site for the formation of hydrogen bridges with γ-Al_2O_3. Al − O − H···OH or Al − O^-···OH long chain could be formed in the suspension [67], which could effectively enhance the coating adhesion. On the other hand, partly dissolved alumina could form Al − O − Al group, which may enhance the particle cohesion during drying. Furthermore, γ-Al_2O_3 particles of small sizes can be easily filled into the space between the large polymer binder particles. Alumina particles could migrate with the shrinking process to the contact points between particles during

Table 1
Effect of binder addition in the slurry on the surface area and adhesion of the γ-Al_2O_3 washcoat on FeCrAlloy platelets.[a]

Slurry composition		pH of the slurry	Surface area[b]	Weight loss[c]
γ-Al_2O_3 (wt%)	Binder (wt%)	(–)	(m^2 g^{-1})	(wt%)
20	Without binder	3.5	101.25	62.5
20	1.6 wt% 2-HEC	3.5	82.78	35.9
20	1.6 wt% Tylose	3.5	82.60	0
20	15 wt% PEG	3.5	74.25	45.2
20	5 wt% PVA	3.5	78.53	0
20	5 wt% PVA + 1 wt% boehmite	3.5	83.10	5.2

[a] Other slurry preparation conditions: γ-Al_2O_3 initial particle size at 3 μm, PVA MW of 146,000–186,000, other binder MW information listed in Section 2.1.
[b] Measured surface area of the γ-Al_2O_3 washcoat based on the BET method.
[c] Weight loss of the washcoat according to the thermal shock test.

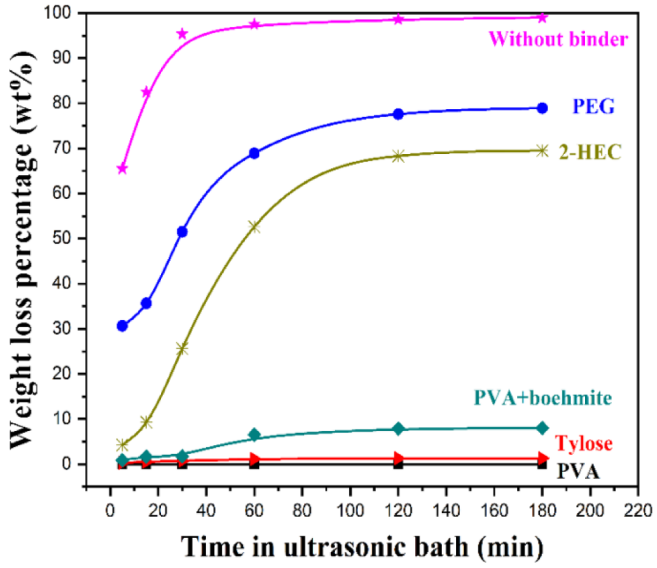

Fig. 2. Weight loss of the washcoated γ-Al_2O_3 layer as a function of the ultrasonic test time and the binder nature. Substrate: FeCrAlloy multi-channel platelet. Other slurry washcoating parameters are shown in Table 1.

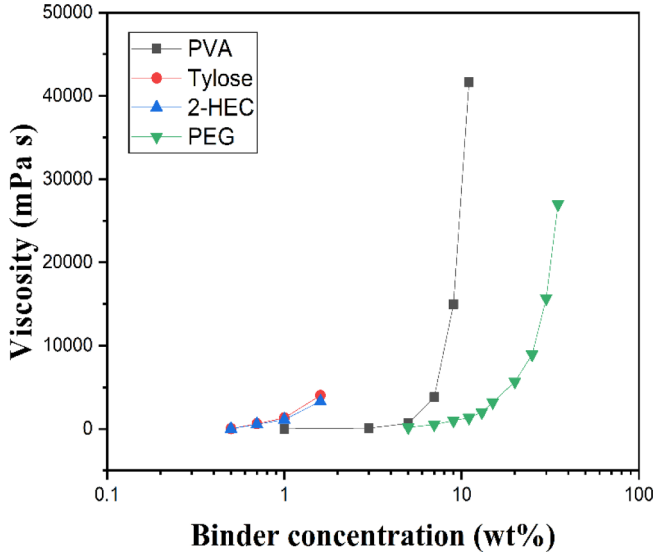

Fig. 3. Slurry viscosity in the presence of different binders (measured at a shear rate of 5 s^{-1}). Slurry preparation conditions: 20 wt% γ-Al_2O_3, pH at 3.5, other details listed in Table 1.

drying, leading to a remarkably increased interlocking between the polymer and alumina. Tylose and PVA have been evaluated to be the best binder considering the negligible weight loss percentage from the ultrasonic and thermal shock tests (Table 1 and Fig. 2). A smaller concentration is required for Tylose than for PVA to achieve the same viscosity (Fig. 3). Also, Tylose is much easier to dissolve in water than PVA. However, the SEM image in Fig. 4a shows some obvious cracks between the side walls and the bottom of the microchannel. The strong shrinkage behavior of Tylose during drying hindered the formation of a smooth and crack-free washcoated layer at the two corners of the rectangular microchannel. In contrast, PVA could be a good option to form a smooth and crack-free washcoated layer, as shown in the SEM image of Fig. 4b.

Although the specific surface area of the obtained washcoat did not vary significantly in the case of adding different binders (Table 1), it was obviously decreased compared with the case without binders. This could be attributed to the modification of the washcoat pore structure to some extent associated with the thermal decomposition of binders during calcination [68,69]. Moreover, binders (e.g. PVA, Tylose, 2-HEC) were completely removed during calcination at ca. 600 °C, as confirmed by TGA results (cf. Fig. B1 in Appendix B). The choice of this calcination temperature throughout the current work for washcoating was also based on the consideration of maintaining an appreciable specific surface area of the γ-Al_2O_3 washcoat (cf. Table B.1 in Appendix B).

3.1.2. Effect of concentration and molecular weight of PVA

As described above, PVA as the binder used in the slurry deposition presents the best washcoat adhesion onto the microchannel wall. The slurry characteristics depend not only on the chemical structure of the binder, but also on its concentration and molecular weight (MW). Higher MW results in an increased slurry viscosity even at low concentrations of PVA (Table 2). The results in Fig. 5 indicate that a stable washcoated layer on the FeCrAlloy platelet with negligible weight loss during the ultrasonic treatment was obtained when using a PVA concentration of 3–5 wt% with the MW at 57,000–186,000, or of 1 wt%, but only with the MW at the highest range tested (146,000–186,000). Upon increasing the MW, longer PVA polymer chains could better disperse alumina particles and better prevent particle agglomeration in the slurry, thus it is possible to provide a better spatial stabilization of alumina in the slurry. However, when the PVA concentration is higher than 5 wt%, the weight loss of the washcoat in the ultrasonic treatment increased obviously with the increasing MW. This could be explained by the fact that a higher MW with a higher concentration commonly results in a stronger shrinkage behavior, which could easily generate cracks on the surface of the finished washcoated layer. Moreover, the excessive polymer binder could occupy a large fraction of the spatial structure in the washcoat than was required, and was not able to form a bond bridge with alumina. The structure was thus much easier to break under high temperature calcination. As for the MW of 13,000–23,000, Fig. 5 shows that the weight loss exhibited an obvious reduction as the PVA concentration was increased from 1 to 11 wt%. The high weight loss at lower PVA concentrations is mainly due to the insufficient amount of polymer and thus less hydrogen bridge links to alumina, especially when considering the fact that a good dispersion of alumina particles in the slurry could not be promoted with such low MW PVA.

In addition, it is seen from Table 2 that the BET surface area of the prepared washcoat layer slightly increased with the PVA MW and concentration. A high surface area might be attributed to a better particle dispersion and less agglomeration using PVA (5 wt%) with a higher MW [70,71]. However, a lower pore volume and average pore size appeared when using a higher PVA MW, possibly due to the disruption of pore structure order with long-chain PVA to some extent [72]. A higher BET surface area obtained at a higher PVA concentration (i.e., at the MW of 88,000–97,000; Table 2) could be explained by the fact that a larger amount of spatial structure was occupied by PVA, which inhibited the close packing of alumina particles. Accordingly, a higher surface area with a larger pore volume and pore size was observed thereof. Thus, the washcoat adhesion and specific surface area could be varied by adjusting the concentration and MW of PVA. Typically, the PVA MW of 57,000–186,000 with the concentration in a range of 3–5 wt% could be considered as an appropriated range for the slurry preparation.

3.1.3. Effect of pH

The pH value determines the fluidity and stabilization of the slurry. PVA with the MW of 146,000–186,000 and concentration of 5 wt% was selected as the optimized binder composition during the slurry preparation. The influence of pH (1.5–9.35) of the slurry was investigated on the weight loss of the finally obtained γ-Al_2O_3 washcoat on FeCrAlloy platelets after 3 h in the ultrasonic bath, as shown in Fig. 6. The weight loss first decreased with the increasing pH value, but then remarkably increased with the pH value reaching 9.35. A distinctive

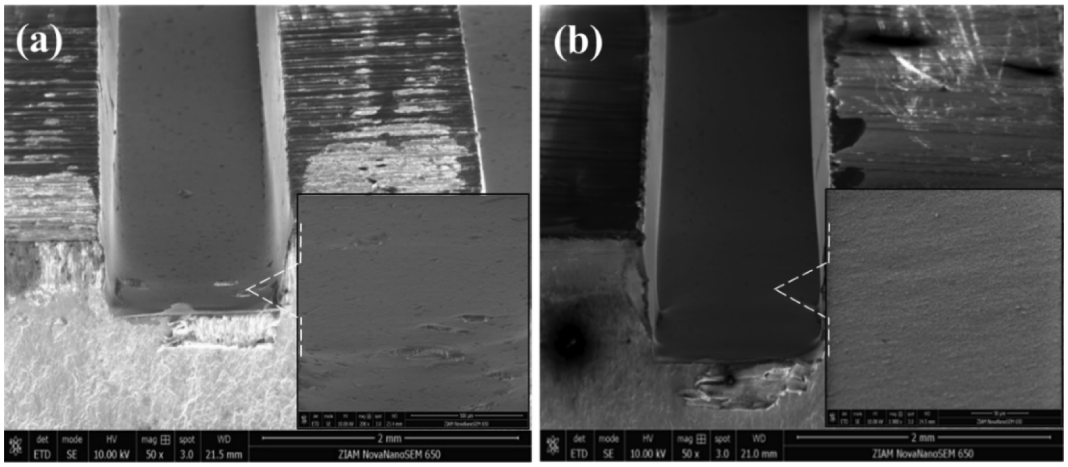

Fig. 4. SEM micrographs of the cross-section of the washcoated γ-Al_2O_3 layer in the microchannel of the multi-channel FeCrAlloy platelet using 1.6 wt% Tylose (a) and 5 wt% PVA (b) as the binder in the slurry. Other slurry washcoating parameters are shown in Table 1.

Table 2
Effect of PVA concentration and molecular weight on the slurry viscosity and the property of the obtained washcoat on FeCrAlloy platelets.[a]

PVA concentration (wt%)	Molecular weight (g mol^{-1})	Viscosity[b] (mPa s)	Surface area[c] (m^2 g^{-1})	Pore volume (cm^3 g^{-1})	Average pore size (Å)
1	88,000–97,000	7.75	64.99	0.32	195.39
5	88,000–97,000	653.10	66.85	0.35	211.43
11	88,000–97,000	36898.20	81.84	0.48	226.92
5	146,000–186,000	784.69	78.53	0.35	198.20
5	13,000–23,000	56.50	62.82	0.45	224.62

[a] Other slurry preparation conditions: γ-Al_2O_3 initial particle size at 3 μm, pH = 3.5.
[b] Measured at a shear rate of 10.34 s^{-1}.
[c] Measured surface area of the γ-Al_2O_3 washcoat based on the BET method.

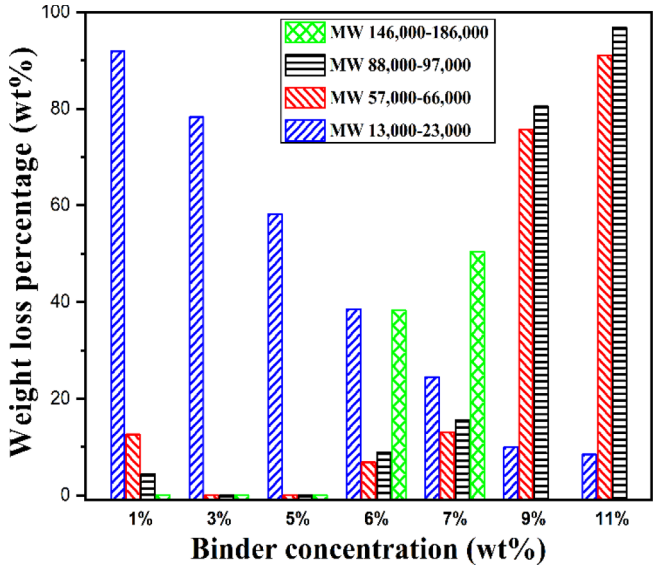

Fig. 5. Weight loss of the washcoated γ-Al_2O_3 layer prepared using PVA as the binder at different concentrations and molecular weights after 3 h ultrasonic treatment. Other slurry preparation conditions: 20 wt% γ-Al_2O_3 (initial particle size at 3 μm), pH = 3.5. Substrate: FeCrAlloy platelet.

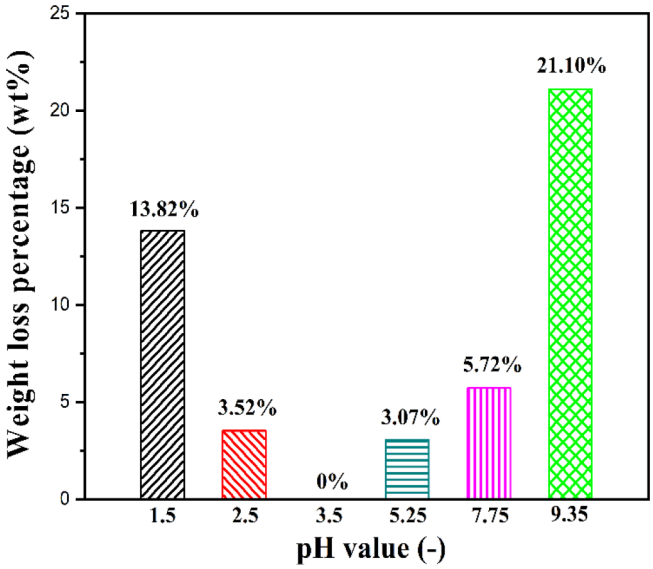

Fig. 6. Weight loss of γ-Al_2O_3 washcoat after 3 h ultrasonic treatment as a function of the pH value of the slurry used for the deposition. Other slurry preparation conditions: 20 wt% γ-Al_2O_3 (initial particle size at 3 μm), 5 wt% PVA (MW of 146,000–186,000). Substrate: FeCrAlloy platelet.

feature may be seen, namely no weight loss at pH = 3.5.

Fig. 7 shows the variation of the slurry viscosity and the zeta potential as a function of the pH value. The viscosity obviously rises, whereas the zeta potential gradually decreases with the increasing pH from 1.5 to 9.35. The larger zeta potential (higher than that of the isoelectric point) indicated that the (negative) particle surface charges increase with the increasing pH. Under a strong base environment, alumina particles in the slurry carry a negative electric charge ($Al_2O_3 + 2OH^- + 3H_2O \rightarrow 2Al(OH)_4^-$). High viscosity values could be explained by the increased adsorption rate of free ions of the negatively charged particles ($Al(OH)_4^-$) over the alumina surface at high pH values [73,74]. The higher amount of free ions carrying more current could remarkably reduce the movement speed of the particles. Thus, an unevenly washcoated layer could be caused by the formation of particle

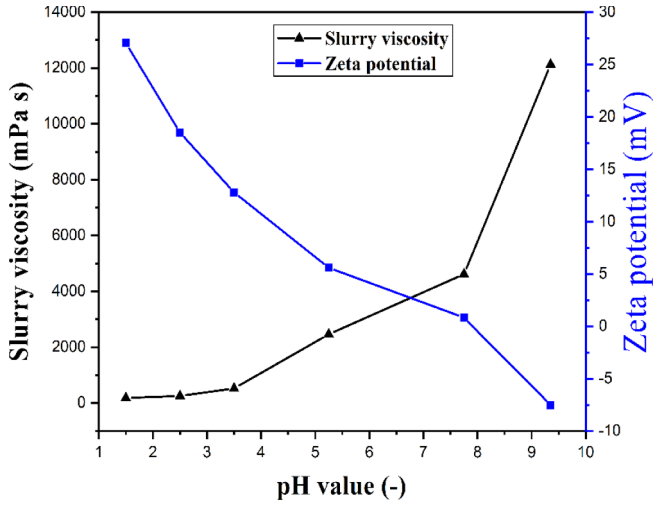

Fig. 7. Slurry viscosity and zeta potential as a function of the pH value. Shear rate for the viscosity measurement was at 10.34 s^{-1}. Other slurry preparation conditions: 20 wt% γ-Al_2O_3 (initial particle size at 3 μm), 5 wt% PVA (MW of 146,000–186,000).

agglomerations and poor particle dispersion at pH = 9.35, as confirmed by the SEM image shown in Fig. 8. This eventually resulted in a high weight loss under the ultrasonic treatment (Fig. 6).

In comparison, low slurry viscosities at lower pH values (< 3.5) resulted in a higher weight loss (Fig. 6). This observation is in good agreement with the tendency of the zeta potential curve (Fig. 7), an important factor to reflect the mobility and stability of the suspension. At lower pH values (e.g., 1.5), the dissolution of alumina particles took place in the acidic solution ($Al_2O_3 + 6H^+ \rightarrow 2Al^{3+} + 3H_2O$)[75]. Al^{3+} dissolution and the surface charging became the main reaction [76]. The mutual electrostatic repulsion forces between particles were enhanced due to the addition of H^+ ions [73,77]. It resulted in a high fluidity of the slurry with well-dispersed alumina particles. Thus at pH < 3.5, a worse coating adhesion was observed when decreasing pH. It is worth noting that the original pH of the prepared slurry was around 5 and the sedimentation took place during storage, and the obtained washcoated layer was also much easier to peel off. Therefore, a stable and uniform washcoated layer of alumina can be formed by preparing slurry at a slight acid environment of pH ≈ 3.5 under which the suitable zeta potential (not too high) and viscosity (not too low) values were ensured.

3.1.4. Effect of initial γ-Al_2O_3 particle size

The weight loss curves of the washcoat subject to the ultrasonic treatment, when using different γ-Al_2O_3 particle sizes in the slurry for deposition on the FeCrAlloy platelet, are presented in Fig. 9a. In the case of particle sizes between 45 and 180 μm, 100 wt% weight loss was found within 1 h, and most of the weight loss took place within 5 min. It seems that the larger the particle size, the higher the weight loss for a given short ultrasonic test time. Here, a serious particle sedimentation in the slurry is expected to have occurred, which could be attributed to the significant liquid–solid density difference. For instance, the slurry prepared with 100 μm alumina exhibited an obvious sedimentation with the appearance of two separate phases within 10 h (Fig. 9b). Thus, the slurry composed of larger particles is generally less adhered onto the substrate than that of smaller particles. Larger γ-Al_2O_3 particles in the suspension are thus not favorable to form the extensive mechanical interlocking due to fewer contact points for anchorage.

As the alumina particle size decreased to 3 μm, more substantial contact points could be created between smaller particles, leading to a significantly improved anchorage and interlocking on the surface of the substrate [5]. Brownian motion usually overcomes the effect of gravity for smaller particles (e.g., with sizes around the sub-micron scale). Thus, no separate phases occurred for alumina with 3 μm even after 3 months (Fig. 9b). However, for the particle size in a range of 0.02 to 3 μm, the washcoat weight loss increased with the decreasing particle size in use (Fig. 9a). The maximum weight loss is 18 wt% after 3 h ultrasonic test in the case of using a particle size of 0.02 μm. As shown in Fig. 9b, for this particle size the sedimentation of the slurry slowly occurred within 4 days (the reason of which is not clear yet). In this case, alumina particles seemed to be loosely bounded due to the weaker interlocking formed between particles in the deposited coating, and eventually could be easily peeled off under the ultrasonic vibration.

Furthermore, smaller particles are more capable of penetrating into the surface cavities, forming a strong interlocked with the substrate. The tighter packing of particles of smaller sizes (e.g., 3 μm), the stronger the mechanical/interfacial force formed between particles and the substrate. However, much larger particles are not favorable to form the extensive mechanical interlocking, due to a looser particle packing that can be easily carried away from the ultrasonic vibration [39].

Interestingly, it has been reported that a good adhesion of CeO_2/CuO washcoat on ceramic monoliths could be achieved starting from a slurry with a ceria particle size range from ca. 1 to 3 μm [78,79]. This size range is similar to our findings, suggesting that the optimal particle size in the slurry for a good adhesion might poorly depend on the chemical composition of the washcoated layer.

All the above observations indicate that the initial γ-Al_2O_3 particle size is an essential factor that affects the adhesion characteristics of the washcoated layer on the substrate. A higher mechanical stability of the washcoated layer can be obtained with relatively smaller initial particle sizes. A γ-Al_2O_3 particle size of about 3 μm seems appropriate for obtaining a well-adhered washcoated layer with endurance.

3.1.5. Effect of γ-Al_2O_3 content

The adhesion test results on the FeCrAlloy platelet under the ultrasonic treatment of washcoats prepared with various γ-Al_2O_3 concentrations in the slurry are presented in Table 3. Almost no weight loss was observed of the washcoat when the γ-Al_2O_3 concentration used was in a range of 10–20 wt%. The weight loss sharply increased to 10.03 wt% and 32.56 wt% when the γ-Al_2O_3 concentrations were at 30 wt% and 40 wt%, respectively. Moreover, the coating surface appeared to have irregularities in the latter cases (Fig. 10). This may be explained by the stronger attractive force caused by a closer distance between alumina particles at high concentrations. The surface cracks consequently

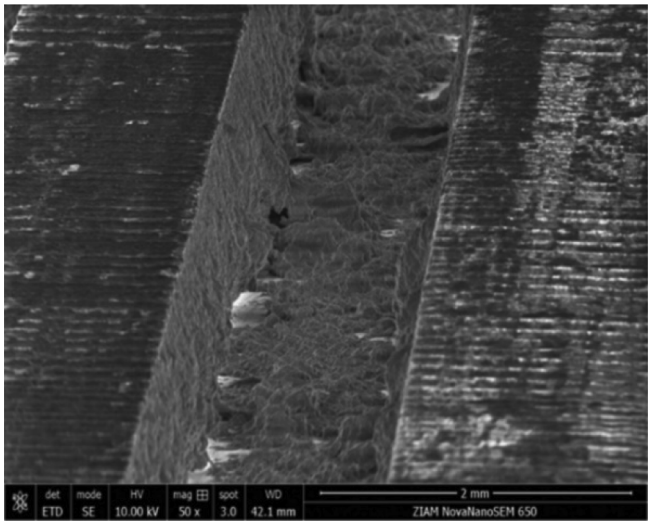

Fig. 8. SEM micrograph of the washcoated γ-Al_2O_3 layer on the microchannel of the FeCrAlloy platelet. Slurry preparation conditions: 20 wt% γ-Al_2O_3 (initial particle size at 3 μm), 5 wt% PVA (MW of 146,000–186,000), pH = 9.35.

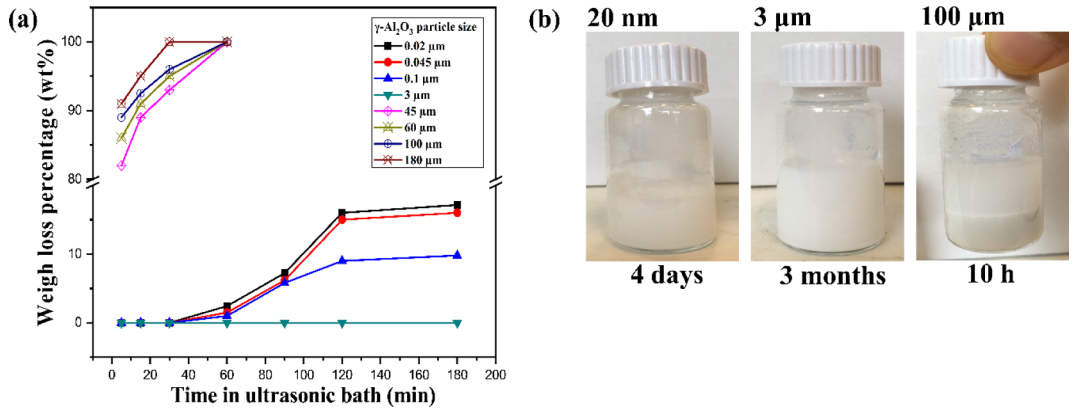

Fig. 9. (a) Weight loss of the washcoated γ-Al_2O_3 layer on the microchannel of the FeCrAlloy platelet as a function of γ-Al_2O_3 particle size used in the slurry preparation. (b) Photos of slurries prepared using 20 nm, 3 μm and 100 μm γ-Al_2O_3 particles at different storage times. Other slurry preparation conditions: 20 wt% γ-Al_2O_3, 5 wt% PVA (MW of 146,000–186,000), pH = 3.5.

appeared during calcination due to the particle agglomeration. Also, the slurry viscosity was found to exponentially increase with the increasing γ-Al_2O_3 concentration. Increasing the slurry viscosity (or γ-Al_2O_3 concentration) and/or the number of washcoated layers tended to increase the γ-Al_2O_3 loading on the microchannel (Table 3). SEM images (Figs. 10a and b) also visually confirm that the γ-Al_2O_3 loading on the microchannel was remarkably increased in the cases of using 30 wt% and 40 wt% γ-Al_2O_3 in the slurry compared with the case with 20 wt% γ-Al_2O_3 (Fig. 4b). The formation of an uneven washcoated layer was observed, however, in the cases with higher γ-Al_2O_3 concentrations (> 20 wt%).

The desired amount of the washcoat to support the catalytically active component on a microchannel commonly depends on the reaction type/conditions and the targeted application. In terms of the single layer loading, it could be increased from 28.01 to 123.97 g m^{-2} when using 10 to 40 wt% γ-Al_2O_3 in the slurry for deposition. Similar observations were reported by several researchers [27,80–82]. To reach a higher amount of the washcoat deposited on the microchannel, successive deposited layers are often needed.

3.1.6. Effect of reactor material and channel shape

Based on the optimal washcoating conditions on FeCrAlloy multichannel platelets found from the experiments discussed above, γ-Al_2O_3 washcoating has been applied onto two different reactor materials (FeCrAlloy and 316 L stainless steel) in the form of capillaries or multichannel platelets with different channel shapes (round, rectangular and square). The coating conditions are characterized by using 20 wt% γ-Al_2O_3 (initial particle size at 3 μm), PVA as the binder (MW of 146,000–186,000), pH = 3.5 in the slurry. No weight loss under the ultrasonic treatment was observed when depositing the washcoated layer on FeCrAlloy substrates with (micro)channels of both round and rectangular shapes (Table 4). In contrast, 0.66 wt%, 8.24 wt% and 11.49 wt% weight losses in the washcoating have been observed for (micro)channels made of stainless steel material with round, rectangular and square shapes, respectively. Under such circumstances, the washcoat detachment mostly occurred at two bottom corners of the rectangular or square channels after the ultrasonic treatment (Fig. 11). The weight loss difference between the two materials is firstly due to that the surface of FeCrAlloy was much rougher than that of stainless steel. Thus, more anchoring sites existed over the FeCrAlloy surface, resulting in a stronger interlocking between the washcoated particles and surface irregularities over the substrate. More importantly, a thin layer of alumina was formed on the FeCrAlloy surface after calcination, which effectively improved the adhesion strength. For the stainless steel case, iron oxide was probably formed on the surface after calcination. It is thus assumed that the washcoated layer possibly has a stronger affinity with the alumina thin layer (e.g., via Al − O − Al bonds) on FeCrAlloy than with iron oxide (e.g., via Al − O − Fe bonds) on stainless steel.

In order to improve the coating adhesion on 316 L stainless steel, the primer coating (cf. details in Section 2.2.2) was employed before depositing alumina coating [17,83]. According to the literature [17,70], a strong bond between the primer coating and the peroxidized 316 L surface could be formed. However, the test results indicate that the use of the current primer coating could not reduce the washcoat weight loss during the ultrasonic treatment (cf. Table C.1 in Appendix C), where 23.84 wt% weight loss was observed on the stainless steel multi-channel platelet for 1 h ultrasonic test. This is even worse than the results without applying primer coating (Table 4). The reason for this is not clear yet, which indicates that the primer coating method deserves further investigation. Thus, the primer coating was not used in our following experiments.

3.1.7. Effect of viscosity during the drying process

The washcoated layer (i.e., as tested on multi-channel platelets of this study) should have a uniform and constant thickness along the

Table 3
Effect of γ-Al_2O_3 concentration on the slurry viscosity, the loading and adhesion strength of the obtained washcoat on FeCrAlloy platelets.[a]

γ-Al_2O_3 concentration (wt%)	Viscosity of slurry (mPa s)[b]	Weight loss percentage[c] (wt%)	γ-Al_2O_3 loading (g m^{-2})			
			1st layer	2nd layer	3rd layer	4th layer
10	273.26	0.11	28.01	68.00	105.60	173.50
20	784.69	0	54.16	110.60	183.50	283.50
30	1652.72	10.03	90.41	198.50	296.50	510.00
40	18121.40	32.56	123.97	305.00	460.60	/

[a] Other slurry preparation conditions: γ-Al_2O_3 initial particle size at 3 μm, 5 wt% PVA (MW of 146,000–186,000, pH = 3.5.
[b] Measured at a shear rate of 10.34 s^{-1}.
[c] Weight loss tested on the single layer washcoat for 3 h ultrasonic treatment.

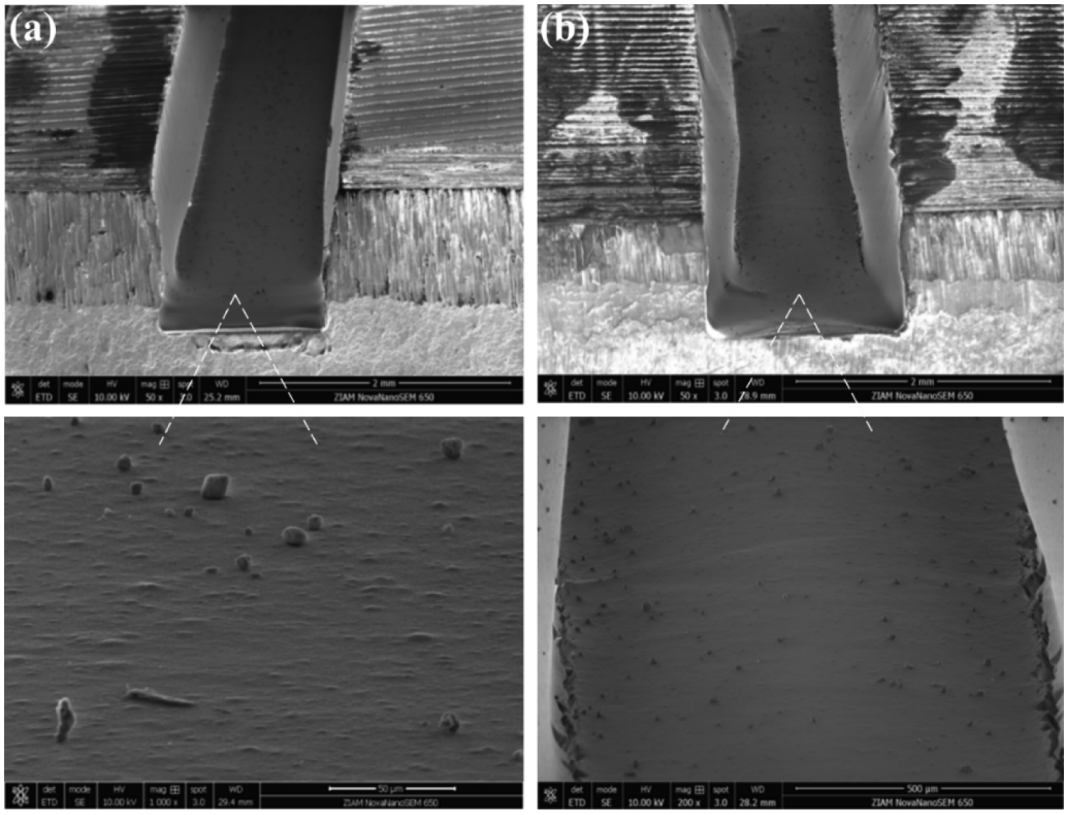

Fig. 10. SEM micrographs of the cross-section of the washcoat in the microchannel of the FeCrAlloy multi-channel platelet using 30 wt% (a) and 40 wt% (b) γ-Al_2O_3 in the slurry. Other slurry washcoating parameters are shown in Table 3.

Table 4
Weight loss of the γ-Al_2O_3 washcoated layer on different reactor materials with different channel shapes after 3 h ultrasonic treatment.[a]

Channel shape	Weight loss percentage (wt%)	
	FeCrAlloy	316 L stainless steel
Rectangular[b]	0	8.24
Circular[c]	0	0.66
Square[c]	Not tested	11.49

[a] Channel dimensions are shown in Section 2.1. Slurry preparation conditions: 20 wt% γ-Al_2O_3 with its initial particle size at 3 μm, 5 wt% PVA (MW of 146,000–186,000), pH = 3.5.
[b] Tested on parallel microchannels in a multi-channel platelet.
[c] Tested in capillaries.

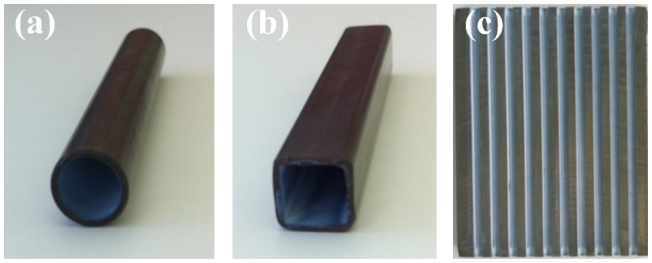

Fig. 11. Washcoated layer on 316 L stainless steel with different channel shapes: (a) circular (d_C = 8 mm), (b) square (width × height × length = 8 × 8 × 100 mm), (c) rectangular (width × height × length = 1.5 × 1 × 50 mm). Slurry preparation conditions are shown in Table 4.

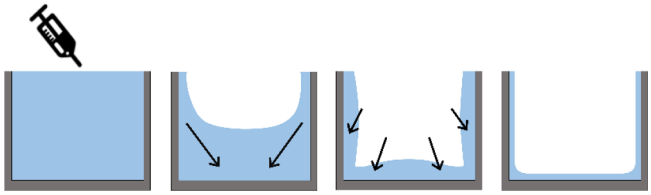

Fig. 12. Schematic of the drying process of the deposited γ-Al_2O_3 slurry in a rectangular microchannel (i.e., on a multi-channel platelet as tested in this study).

microchannel, for ensuring its good catalytic performance when impregnated with catalytically active components. The platelets were initially fully filled with the slurry. The excess slurry around the top of parallel microchannels was then scraped off. The slurry adhered to the bottom and the side walls of microchannels during drying. The drying process was characterized by the particle packing and the shrinkage degree, which is supposed to rationalize the washcoat shape as shown in Fig. 12. The water evaporation in the washcoated layer is accompanied by the shrinkage behavior at the same time. During the experiment, it was observed that drying of highly viscous suspensions was faster to reach the finally stagnant film (due to less volatility) compared with suspensions with low viscosity. That is, in the latter case, a longer drying time was needed to reach the stagnant film for the same γ-Al_2O_3 loading. The film thickness further shrunk until a homogeneous solid washcoated layer was formed. For less viscous suspensions, part of the suspension at the top section of side channel walls may slowly slip

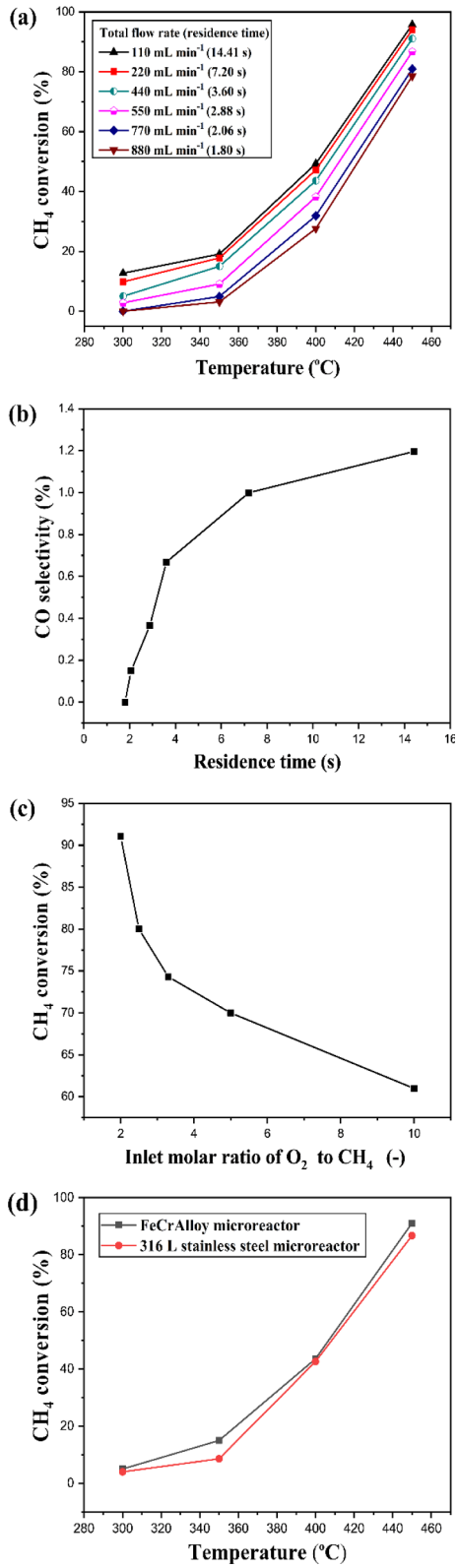

Fig. 13. Catalytic methane combustion over the coated Pt/γ-Al_2O_3 catalyst in the multi-channel microreactor with (a-c) FeCrAlloy platelets (3.8 wt% Pt loading) and (d) FeCrAlloy or stainless steel platelets (3.5 wt% Pt loading). (a) Methane conversion under different reaction temperatures and flow rates, $\Phi = 2$. (b) CO selectivity under different residence times at 450 °C and $\Phi = 2$. (c) Methane conversion under different inlet O_2/CH_4 molar ratios at 450 °C; the air flow rate at 400 mL min^{-1}. (d) Methane conversion under different reaction temperatures, for a total flow rate at 440 mL min^{-1} and $\Phi = 2$. Loadings of Pt/γ-Al_2O_3 in the FeCrAlloy and 316 L stainless steel microreactors are 80.8 and 74.4 g m^{-2}, respectively.

down and accumulate at the bottom of the channels during drying. The coating layer thus appeared to be thicker on the bottom than on the two side walls. In contrast, the washcoated layer in the case of using highly viscous suspensions was much thicker at the lower part of the side walls than at the upper part. Thus, a suitable slurry viscosity is required for a uniform coating around the microchannel, which is in qualitative agreement with SEM images shown in Figs. 4b and 10).

3.2. Catalytic methane combustion over the coated Pt/γ-Al_2O_3 catalyst in the multi-channel microreactor

The catalytic methane combustion was studied over the coated Pt/γ-Al_2O_3 catalyst in the multi-channel microreactor (containing the microchannel platelet made of FeCrAlloy or 316 L stainless steel). The coating was applied using the optimized slurry preparation conditions characterized by using 20 wt% γ-Al_2O_3 (3 μm particle size), 5 wt% PVA (MW of 146,000–186,000) at a slurry pH of 3.5, followed by the impregnation of Pt. The TEM picture confirms the successful dispersion of platinum particles in the catalyst (cf. Fig. D.1 in Appendix D). The reaction performance as a function of the key operational conditions was investigated, including the temperature, flow rate and O_2/CH_4 molar ratio. The temperature distribution along the microreactor was also studied under selected reaction conditions.

3.2.1. Effect of operating conditions on the methane conversion

The methane conversion as a function of the reaction temperature under different total flow rates (i.e., the sum of air and methane flow rates, based on ca. 20 °C and 1 atm) is shown in Fig. 13a, for the multi-channel microreactor composed of FeCrAlloy platelet. At a total flow rate of 110 mL min^{-1}, the conversion presented a remarkable increase from 12.7% to 95.75% when the temperature was increased from 300 to 450 °C at an inlet O_2 to CH_4 molar ratio (Φ) of 2. The light-off was observed with a sharp conversion increase starting at ca. 350 °C. This light-off phenomenon is likely due to the local heating of the catalyst given the highly exothermic nature of the combustion reaction (the heat of the reaction, ΔH_R being ca. −810 kJ mol^{-1}) and the favorable fractional coverage of the catalyst surface by the adsorbed methane and oxygen under such conditions [47,48], leading to a significant increase of the catalytic activity. The smaller flow rate rendered a longer residence time (τ; cf. Eq. (4)) in the coated microchannel. For instance, the residence time was increased by a factor of 8 from 1.8 s (880 mL min^{-1}) to 14.41 s (110 mL min^{-1}) at 450 °C, and thus the methane conversion was increased from 78.53% to 95.75%. Fig. 13a further reveals that the reaction temperature has a greater influence than the flow rate, due to the remarkable increase of the intrinsic kinetic rate especially at the catalytic ignition temperature (where the light-off occurs) or above.

Fig. 13b shows that carbon monoxide was formed increasingly when prolonging the residence time ($\tau > 1.8$ s) at a reaction temperature of 450 °C and $\Phi = 2$ (stoichiometric ratio for a complete combustion), however, its selectivity is low (< 1.2%). One possibility for CO formation is that the adsorbed oxygen over the localized areas of the catalyst was not sufficient [48], giving rise to the incomplete combustion ($CH_4 + 1/2O_2 \rightarrow CO + 2H_2$). Moreover, H_2 produced herein could further react with the complete combustion product, CO_2, according to the reverse water–gas shift reaction to produce CO ($H_2 + CO_2 \rightarrow CO + H_2O$). It seems from Fig. 13b that the longer the residence time, the higher the chance for such reactions for CO formation to occur. It should be noted that no carbon monoxide was detected (i.e., the CO_2 selectivity being 100%), when Φ was set higher than 2, indicating a more sufficient coverage of the adsorbed oxygen on the catalyst surface.

Fig. 13c reveals that the methane conversion tended to decrease when increasing Φ from 2 to 10 (oxygen-rich). The lower conversion for the oxygen-rich case could be explained by the competitive adsorption between oxygen and methane over the catalyst surface. Since the

methane adsorption energy is higher than that of oxygen [84], a competitive adsorption of oxygen prevented further oxidation by inhibiting the weakly adsorbed methane on the active sites [85]. Thus, a favorable surface coverage by the adsorbed methane and oxygen over the catalyst surface is essential for achieving a desired conversion. Another possibility is that the bond between the absorbed oxygen and the oxidized platinum is stronger than that with metallic platinum [86], which is not favorable for methane and/or oxygen adsorption (rate determining step). Commonly, its metallic state presents a higher catalytic activity compared to its oxidized state (PtO_2), despite the high-dispersed phase of the latter state [87,88]. Thus, the platinum catalyst itself might be less active under the condition of the predominant oxygen-covered surface and thus not be able to fully catalyze methane oxidation especially when the present methane amount was high. Consequently, a low methane conversion would be expected when using an oxygen-rich mixture due to the insufficient adsorbed methane and/or less available metallic state of platinum on the catalyst surface.

Fig. 13d presents a comparison of the methane conversion in the multi-channel microreactors composed of FeCrAlloy and 316 L stainless steel reaction platelets. A slight lower conversion was obtained in the stainless steel microreactor under otherwise the same conditions, possibly due to a somewhat lower Pt loading. Considering the coating adhesion strength, FeCrAlloy microreactors appear to be a better option for long-term uses, whereas 316 L stainless steel microreactors represent a more cost-effective alternative (especially if the coating adhesion is better addressed).

3.2.2. Effect of operating conditions on the microreactor temperature distribution

The temperature distribution along the multi-channel microreactor (with FeCrAlloy platelets) was measured during the catalytic methane combustion, using the thermocouples that touched the top of the middle microchannel on the platelet. A blank experiment for temperature measurement was also conducted with only air flowing through the microreactor, as a reference case for comparison.

It was observed in Fig. 14a that for a reaction temperate (i.e., the oven temperature) at 450 °C, the temperature along the microchannel was close to uniform in the reference case without reaction occurrence. Temperature values close to the middle of the microchannel appeared to be slightly higher than those at both ends, with a difference below ca. 5 °C. This is mainly a result of the oven temperature profile. Once the reaction started, such a (close to) uniform temperature profile was no longer sustained in the microchannel. For a total flow rate at 440 mL min^{-1} and $\Phi = 2$ (Fig. 14a), the temperature in the front part of the microchannel increased more significantly (e.g., at the normalized length of the microchannel, $L^* = 0.2$), due to the released combustion reaction heat and the location of the reaction front in the middle section or further upstream (*vide infra*). At a given axial location, the temperature was gradually increased upon increasing the reaction test time on stream until 50 min, after which the temperature reached a stable state showing the thermal inertia of the microreactor. Moreover, the temperature was increased mainly in the front part, and then was gradually decreased to the trailing end of the microchannel. It may be concluded that the majority of methane was converted at the front section of the microreactor. And (much) less reaction took place at the latter section of the microreactor under these conditions, resulting in a somewhat insignificant temperature increase therein.

The effect of flow rate on the temperature distribution along the microreactor is illustrated in Fig. 14b. More heat would be released at a higher total flow rate due to the more involved methane, despite a slightly lower methane conversion (Fig. 13a). Thus, the temperature was noticeably raised along the microreactor at higher flow rates (Fig. 14b), and the axial location with the peak temperature seems to gradually move downstream along the microreactor. This is due to a shorter residence time at a higher flow rate, implying that more methane was converted at a longer distance from the microchannel inlet.

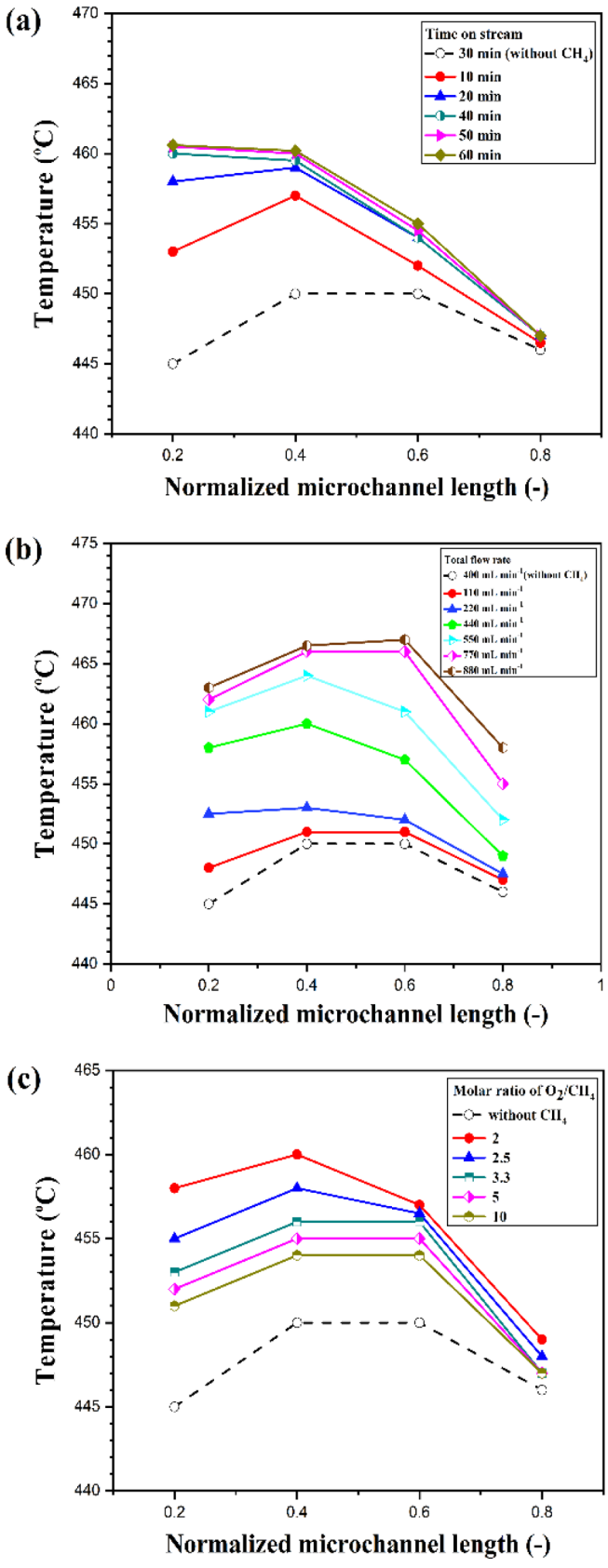

Fig. 14. Axial surface temperature distribution during the catalytic methane combustion in the multi-channel microreactor (with FeCrAlloy platelets). The oven temperature was fixed at 450 °C as the reported reaction temperature. (a) Effect of time on stream; the total flow rate at 440 mL min^{-1}, $\Phi = 2$. (b) Effect of the total flow rate, $\Phi = 2$ (c) Effect of the inlet O_2/CH_4 molar flow ratio; the air flow rate at 400 mL min^{-1}. In (b) and (c), data were collected after 30 min on stream.

This is in line with the literature observation during the catalytic combustion of methane over monolithic catalysts based on (Pt-)$LaMnO_3$ that the reaction front shifted upstream along the channel at a longer residence time [89,90]. At the reaction front, the fluid has reached the catalytic ignition temperature resulting a large reaction heat release and consequently a sharp increase in the fluid/catalyst temperature [91]. The remaining length of the reactor after the reaction front experienced either no reaction or an insignificant conversion, thus this part acted mainly as a heat exchanger and the fluid/catalyst was cooled down due to external heat losses [89–91]. With the increasing flow rate, it tends to take a longer distance to heat the reactant mixture to the ignition temperature, resulting a downstream shift of the reaction front.

Similarly, the concentration variation of the adsorbed methane and oxygen over the catalyst surface significantly affected the temperature distribution. The obvious temperature gradient over the microreactor in this case can be observed in Fig. 14c. Both the methane conversion and the temperature increase could achieve a maximum at a stoichiometric ratio of 2 (cf. Fig. 13c as well). With the increasing inlet O_2/CH_4 molar ratio, the temperature in the microreactor at a given axial location was obviously decreased, an observation in line with the reduced methane conversion shown in Fig. 13c. Under such circumstances, there is less thermal power provided via combustion, and possibly less favorable surface coverage over the catalyst surface due to the competitive adsorption between oxygen and methane (as discussed in Section 3.2.1), leading to a temperature or conversion decrease. Apart from that, another reason for the lower temperature under the oxygen-rich conditions (at $\Phi > 2$) is that more balance gas (nitrogen) was involved. Thus, a part of the released heat was diluted and absorbed by the balance gas.

The actual maximum value present in the temperature profile and its position in the reactor (as shown in Figs. 14a–c) depend significantly on the pre-heating temperature, the thermal power of the reactant mixture (i.e., related to its composition and flow rate), as well as the heat losses of the reactor (realized in the current work via the conduction through the microreactor wall to the oven atmosphere). Moreover, in our experiments the temperature was only measured on the top surface of the middle microchannel (without coating), since the tips of thermocouples (o.d.: 3 mm) are not possible to touch the inner catalytic wall (Fig. 1). Thus, the temperature level and profile reported in this work are only indicative of that on the catalyst surface. Considering the good thermal conductivity of FeCrAlloy platelets and the reaction heat released, the actual surface temperature of the catalyst should be much higher than these measurements. To illustrate, the adiabatic temperature rise (ΔT_{ad}) can amount to ca. 2000 °C at $\Phi = 2$ (calculations not shown for brevity) [92]. Thus, it is reasonable to estimate that the actual temperature on the catalyst surface could be somewhat high under the present reaction conditions, which might accelerate the catalyst deactivation as well [93]. The high temperature level on the catalyst surface could also activate and thermally sustain the homogeneous combustion to a certain extent, as addressed in many literatures [89,90,93–95]. Investigation of the above-mentioned aspects would contribute to optimized operating conditions and microreactor design for the catalytic methane combustion. These findings, when coupled with heat transfer studies (e.g., in the presence of the integrated heat exchanging modules), can provide insights into the potential uses of such wall-coated microreactors in energy-related applications (e.g., for heat supply in a small-scale boiler system [96]).

3.2.3. Preliminary results of catalyst deactivation

Catalyst life is an important indicator for its performance, especially relevant to the long-term operation in the commercial applications. Regarding the coated Pt/γ-Al_2O_3 catalyst in the multi-channel microreactors, a detailed in-situ life time study has not been performed yet. However, the coated Pt/γ-Al_2O_3 catalyst scrapped from the stainless steel substrate has been tested in the powder form in a fixed bed reactor for 100 h on stream. A somewhat significant decrease of the catalyst activity was already noticed (see Appendix E for more details). This deactivation is possibly due to the catalyst sintering and the growth of Pt particles (e.g., as a result of the high temperature level generated by the released heat at the reaction front), or the formation of platinum species in the oxidized state (PtO_2) with a lower activity compared to its metallic state [97–99]. These preliminary results imply that the catalyst coating preparation in microreactors still needs to be further optimized (e.g., by improving the catalyst structural stability and the metal-support interaction), together with the catalyst regeneration, in order to maintain a stable catalyst activity.

4. Conclusions

In this work, the slurry washcoating followed by the incipient wetness impregnation has been used to prepare Pt/γ-Al_2O_3 catalytic coatings in microreactors. The effect of various factors in the slurry preparation procedures on the adhesion properties (tested typically via the ultrasonic treatment) of the washcoated γ-Al_2O_3 layer on the microreactor substrates with different channel shapes was investigated. The initial γ-Al_2O_3 particle size and pH were found as two important factors affecting the slurry stability and the washcoat adhesion strength. A strong particle attractive force could be maintained by using a particle size of around 3 μm in the slurry with a slightly acid environment (pH ≈ 3.5). PVA (typically at a concentration of 3–5 wt% and a MW of 57,000–186,000) was identified as a suitable binder to better disperse alumina particles and form sufficient hydrogen bridges with alumina, thus effectively enhancing the washcoat adhesion. FeCrAlloy as the (micro)reactor substrate exhibited an excellent coating adhesion with negligible weight loss during the ultrasonic treatment in either rectangular or round channels, primarily because of the formation of alumina film over the surface during thermal pretreatment. In contrast, 316 L stainless steel as the substrate only showed a relatively good adhesion in a round channel, presumably due to the lack of a strong chemical bonding between the washcoated layer and the pretreated substrate surface.

The catalyst performance in the catalytic methane combustion was further examined in microreactors comprising parallel microchannels made of FeCrAlloy or 316 L stainless steel. A higher total flow rate (of methane and air) was found to render higher heat generation rate and lead to a more significant temperature increase in the front part of the microreactor, despite a slightly decreased methane conversion due to a shorter residence time. Under the oxygen-rich conditions, the predominant adsorption of oxygen over methane species on the catalyst surface could lead to a decreased methane conversion and thus a lower heat generation. Thus, an appropriate fractional coverage of the catalyst surface by these species and a proper reaction condition selection are needed for achieving the favorable methane conversion, as well as the sufficient heat release for the potential uses of such microreactors for energy-related applications. Somewhat significant deactivation of the coated Pt/γ-Al_2O_3 catalyst over a time scale of 100 h, as observed in an ex-situ test in a fixed-bed reactor, represents a further direction of improvement to be addressed in our future work.

Acknowledgements

The authors are grateful for the financial support from the University of Groningen (start-up package in the area of green chemistry and technology for Jun Yue, and Ubbo-Emmius Fund 2015). This work was also financially supported by the University of Nantes, Region Pays de la Loire (Chaire Connect Talent ODE). The authors thank the technical support from Gwenaël Biotteau and Nicolas Lefevre at the University of Nantes, Erwin Wilbers, Marcel de Vries, Léon Rohrbach and Daniël Vreugdenhil at the University of Groningen.

Appendix A

Washcoating of γ-Al_2O_3 inside a capillary

For coating inside circular or square capillaries, a certain mass of the γ-Al_2O_3 slurry was injected inside via a syringe. One end of the coated capillary was then connected with the motor which rotated at a given speed (Fig. A.1). During drying, the connection was switched from one to the other end of the capillary multiple times. Thus, the slurry near the open end side of the capillary was faster to be dried, whereas that in the middle of the capillary could be the last part to be dried. However, some imprints like 'tree-rings' may be observed on the washcoated layer after drying. Thus, a better method to dry the coating inside such capillaries might be to directly heat it up to a certain temperature in the oven with a low loading of alumina, so as to reduce the gravity influence. More alumina loading could be achieved by multilayer coating with the same method.

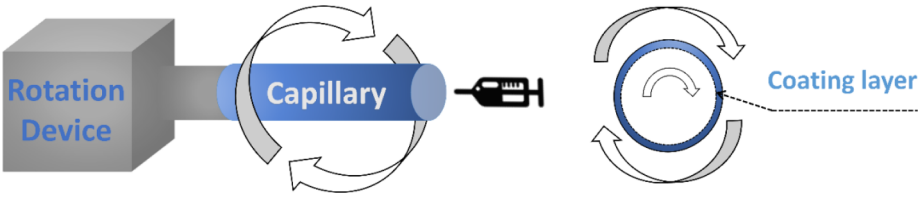

Fig. A.1. Schematic of the drying process of the deposited γ-Al_2O_3 slurry in a circular capillary.

Appendix B

TGA analysis of the slurry

The amount of slurries (prepared under the conditions mentioned in Table 1) for TGA analysis is 3–10 mg. The results of analysis in the case of using different binders are shown in Fig. B.1, together with the first derivation of the TGA curve (DTG). The first weight loss (< 100 °C) is ascribed to the desorption of the physically adsorbed water in the slurry. The second weight loss (at 200–300 °C) and third one (at 400–500 °C) are associated with the thermal decomposition of binders. This indicates that binders were completely decomposed when being calcined at 600 °C. However, the specific surface area of the obtained washcoat decreased with the increasing calcination temperature due to the structure damage of alumina (e.g., pore collapse), as shown for the case of PVA as the binder in Table B.1. Considering both the specific surface area and the binder removal, 600 °C was chosen as a suitable calcination temperature.

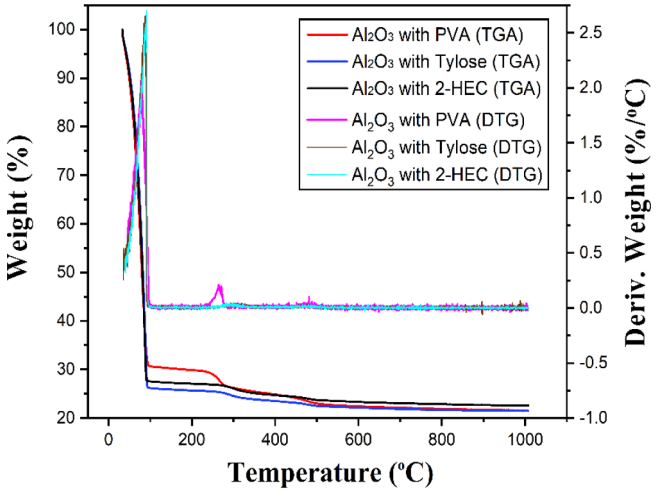

Fig. B.1. TGA and DTG curves of slurries prepared under the conditions mentioned in Table 1.

Table B.1
BET surface area and pore properties of the washcoated γ-Al_2O_3 layer obtained on FeCrAlloy platelets under different calcination temperatures.[a]

Calcination temperature (°C)	BET surface area ($m^2 g^{-1}$)	Micropore area ($m^2 g^{-1}$)	Pore volume ($cm^3 g^{-1}$)	Average pore size (Å)
800	54.05	0.51	0.41	277.78
700	61.81	1.40	0.38	200.44
600	78.53	1.73	0.35	198.20
500	86.24	4.39	0.31	160.43

[a] Slurry preparation conditions: 20 wt% γ-Al_2O_3 (initial particle size at 3 μm), 5 wt% PVA as the binder (MW of 146,000–186,000), pH = 3.5.

Appendix C

Effect of primer coating on the adhesion of the γ-Al_2O_3 washcoated layer

Table C.1 shows the weight loss in the ultrasonic treatment of the γ-Al_2O_3 washcoat obtained via applying the primer coating (details shown in Section 2.2.2), followed by the slurry deposition (other preparation conditions are the same as shown in Table 4) on the 316 L stainless steel multi-channel platelet. The weight loss was found to increase to a somewhat significant level upon increasing the treatment time from 5 to 60 min.

Table C.1
Effect of primer coating on the adhesion of the γ-Al_2O_3 washcoated layer on the 316 L stainless steel multi-channel platelet.

Primer composition	Slurry composition[a]	Ultrasonic bath time (min)	Weight loss percentage (wt %)
10 wt% dispersal P2 + 3 wt% PVA	20 wt% γ-Al_2O_3 + 5 wt% PVA	5	0.66
		15	10.76
		30	16.56
		60	23.84

[a] Other preparation conditions are shown in Table 4.

Appendix D

TEM analysis of Pt/γ-Al_2O_3 catalyst

3.5 wt% Pt/γ-Al_2O_3 catalyst was prepared on the FeCrAlloy platelet (with 10 parallel microchannels; see Section 2.1 for dimensions), according to the procedures described in Section 2.2. Herein, the slurry for coating was prepared using 20 wt% Al_2O_3 (3 μm), 5 wt% PVA (MW of 146,000–186,000) and pH at 3.5. Then, the catalyst was scrapped off from the substrate and ground to a particle size below 25 μm. After ultrasonication in acetone for 10 min, the sample was dropped onto the carbon coated copper grid (400 mesh) for TEM analysis. The TEM image is shown in Fig. D.1. Pt particles (black dots) seemed to be well dispersed over the alumina support by using the incipient wet impregnation method.

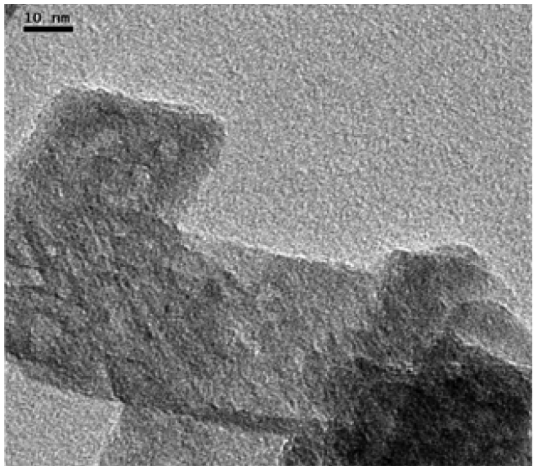

Fig. D.1. TEM image of the 3.5 wt% Pt/γ-Al_2O_3 catalyst scrapped from the FeCrAlloy platelet.

Appendix E

Catalyst life time test in a fixed-bed reactor

3.5 wt% Pt/γ-Al_2O_3 catalyst was prepared on the 316 L stainless steel platelet (with 16 parallel microchannels; see Section 2.1 for dimensions), using the same protocol as mentioned in Appendix D. The fresh Pt/γ-Al_2O_3 catalyst was then scraped from the platelet and ground to a particle size of about 25 μm for the catalyst life time test in a fixed-bed reactor made of glass (U shape; i.d.: 5 mm) in a similar oven and experimental setup as shown in Fig. 1. A full methane conversion was achieved at 450 °C with 16 h on stream (Fig. E.1). However, the catalyst gradually deactivated, with the methane conversion being dropped to 98.12% at 22 h, and 84.61% at 100 h. The CO_2 selectivity also seems to drop slowly over time. The measured BET surface areas of the fresh and used (after 100 h on stream) catalysts are listed in Table E.1. An obvious reduction in the specific surface area of the used catalyst was observed, possibly due to the catalyst sintering after a long-term reaction. Meanwhile, the growth of Pt particles due to agglomeration could also have occurred, which would result in a catalyst activity loss [100–102]. Hence, the current catalyst preparation method still needs to be further improved to maintain a stable catalyst activity.

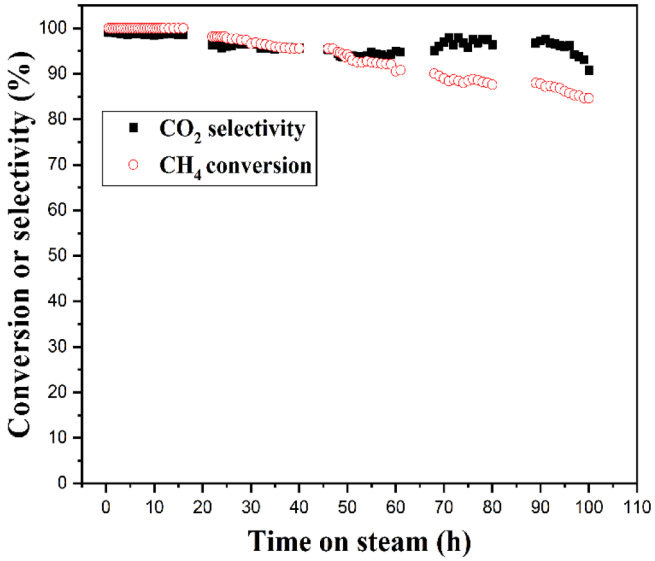

Fig. E.1. Catalyst life time test in a fixed-bed reactor (i.d.: 5 mm). Other conditions: 3.5 wt% Pt/γ-Al_2O_3 catalyst (scrapped from the 316 L stainless steel platelet; 0.2 g; size at ca. 25 μm;), total gas flow rate (of air and methane) at 20 mL min^{-1}, 2.513% CH_4 in the air (Φ = 7.8), 450 °C.

Table E.1
BET surface area of the fresh and used Pt/γ-Al_2O_3 catalysts.

Catalyst	BET surface area ($m^2 g^{-1}$)	Micropore area ($m^2 g^{-1}$)	Pore volume ($cm^3 g^{-1}$)	Average pore size (Å)
Fresh Pt/γ-Al_2O_3	66.07	0.20	0.41	249.42
Used Pt/γ-Al_2O_3[a]	52.38	/	0.40	305.70

[a] After 100 h reaction test (cf. Fig. E.1).

References

[1] D. Van Herk, P. Castano, M. Makkee, J.A. Moulijn, M.T. Kreutzer, Catalyst testing in a multiple-parallel, gas-liquid, powder-packed bed microreactor, Appl. Catal. A 365 (2009) 199–206, https://doi.org/10.1016/j.apcata.2009.06.010.

[2] A. Karim, J. Bravo, D. Gorm, T. Conant, A. Datye, Comparison of wall-coated and packed-bed reactors for steam reforming of methanol, Catal. Today 110 (2005) 86–91, https://doi.org/10.1016/j.cattod.2005.09.010.

[3] W. Ehrfeld, V. Hessel, H. Löwe, Microreactors: new technology for modern chemistry, Wiley, Michigan, 2000.

[4] J. Klaus, H. Volker, L. Holger, B. Manfred, Chemistry in microstructured reactors, Angew. Chem. Int. Ed. 43 (2004) 406–446, https://doi.org/10.1002/anie.200300577.

[5] L.A. Truter, P.R. Makgwane, B. Zeelie, S. Roberts, W. Böhringer, J.C.Q. Fletcher, Washcoating of H-ZSM-5 zeolite onto steel microreactor plates-filling the void space between zeolite crystallite agglomerates particles, Chem. Eng. J. 257 (2014) 148–158, https://doi.org/10.1016/j.cej.2014.07.047.

[6] B. Schmidt, M. Liauw, Mass transfer limitations in microchannel reactors, Catal. Today 110 (2005) 15–25, https://doi.org/10.1016/j.cattod.2005.09.019.

[7] P.L. Mills, D.J. Quiram, J.F. Ryley, Microreactor technology and process miniaturization for catalytic reactions-a perspective on recent developments and emerging technologies, Chem. Eng. Sci. 62 (2007) 6992–7010, https://doi.org/10.1016/j.ces.2007.09.021.

[8] M. Rahimpour, M. Dehnavi, F. Allahgholipour, D. Iranshahi, S. Jokar, Assessment and comparison of different catalytic coupling exothermic and endothermic reactions: a review, Appl. Energy. 99 (2012) 496–512, https://doi.org/10.1016/j.apenergy.2012.04.003.

[9] J. Yue, R. Boichot, L. Luo, Y. Gonthier, G. Chen, Q. Yuan, Flow distribution and mass transfer in a parallel microchannel contactor integrated with constructal distributors, AIChE J. 56 (2010) 298–317, https://doi.org/10.1002/aic.11991.

[10] X. Guo, Y. Fan, L. Luo, Multi-channel heat exchanger-reactor using arborescent distributors: a characterization study of fluid distribution, heat exchange performance and exothermic reaction, Energy 69 (2014) 728–741, https://doi.org/10.1016/j.energy.2014.03.069.

[11] A. Günther, K.F. Jensen, Multiphase microfluidics: from flow characteristics to chemical and materials synthesis, Lab Chip 6 (2006) 1487–1503, https://doi.org/10.1039/B609851G.

[12] V. Meille, Review on methods to deposit catalysts on structured surfaces, Appl. Catal. A. 315 (2006) 1–17, https://doi.org/10.1016/j.apcata.2006.08.031.

[13] V. Paunovic, V. Ordomsky, M.F. Neira D'Angelo, J.C. Schouten, T.A. Nijhuis, Catalyst coating on prefabricated capillary microchannels for the direct synthesis of hydrogen peroxide, Ind. Eng. Chem. Res. 54 (2015) 2919–2929, https://doi.org/10.1021/ie504762y.

[14] V. Hessel, P. Angeli, A. Gavriilidis, H. Löwe, Gas-liquid and gas-liquid-solid microstructured reactors: contacting principles and applications, Ind. Eng. Chem. Res. 44 (2005) 9750–9769, https://doi.org/10.1021/ie0503139.

[15] J. Yue, Multiphase flow processing in microreactors combined with heterogeneous catalysis for efficient and sustainable chemical synthesis, Catal. Today 308 (2018) 3–19, https://doi.org/10.1016/j.cattod.2017.09.041.

[16] M. Liauw, M. Baerns, R. Broucek, O. Buyevskaya, J. Commenge, J. Corriou, L. Falk, K. Gebauer, H. Hefter, O. Langer, Periodic operation in microchannel reactors, Microreaction technology: industrial prospects. Springer, Berlin, 2000, pp. 224-234.

[17] N.R. Peela, A. Mubayi, D. Kunzru, Washcoating of γ-alumina on stainless steel microchannels, Catal. Today 147 (2009) S17–S23, https://doi.org/10.1016/j.cattod.2009.07.026.

[18] R. Zapf, C. Becker-Willinger, K. Berresheim, H. Bolz, H. Gnaser, V. Hessel, G. Kolb, P. Löb, A.K. Pannwitt, A. Ziogas, Detailed characterization of various porous alumina-based catalyst coatings within microchannels and their testing for methanol steam reforming, Chem. Eng. Res. Des. 81 (2003) 721–729, https://doi.org/10.1205/026387603322302887.

[19] X. Xu, H. Vonk, A. Cybulski, J.A. Moulijn, Alumina washcoating and metal deposition of ceramic monoliths, Stud. Surf. Sci. Catal., Elsevier (1995) 1069–1078.

[20] K. Haas-Santo, M. Fichtner, K. Schubert, Preparation of microstructure compatible porous supports by sol-gel synthesis for catalyst coatings, Appl. Catal. A 220 (2001) 79–92, https://doi.org/10.1016/S0926-860X(01)00714-1.

[21] M.P. Vorob'eva, A.A. Greish, A.V. Ivanov, L.M. Kustov, Preparation of catalyst carriers on the basis of alumina supported on metallic gauzes, Appl. Catal. A 199 (2000) 257–261, https://doi.org/10.1016/S0926-860X(99)00563-3.

[22] K.S. Yang, Z. Jiang, J. Shik Chung, Electrophoretically Al-coated wire mesh and its application for catalytic oxidation of 1,2-dichlorobenzene, Surf. Coat. Technol. 168 (2003) 103–110, https://doi.org/10.1016/S0257-8972(02)00569-8.

[23] M. Karches, M. Morstein, P. Rudolf von Rohr, R.L. Pozzo, J.L. Giombi, M.A. Baltanás, Plasma-CVD-coated glass beads as photocatalyst for water decontamination, Catal. Today 72 (2002) 267–279, https://doi.org/10.1016/S0920-5861(01)00505-3.

[24] T. Aaltonen, M. Ritala, T. Sajavaara, J. Keinonen, M. Leskelä, Atomic layer deposition of platinum thin films, Chem. Mater. 15 (2003) 1924–1928, https://doi.org/10.1021/cm021333t.

[25] L.L. Pranevicius, P. Valatkevicius, V. Valincius, C. Montassier, Catalytic behavior of plasma-sprayed Al-Al_2O_3 coatings doped with metal oxides, Surf. Coat. Technol. 125 (2000) 392–395, https://doi.org/10.1016/S0257-8972(99)00584-8.

[26] L. Pranevicius, L.L. Pranevicius, P. Valatkevicius, V. Valincius, Plasma spray deposition of Al-Al_2O_3 coatings doped with metal oxides: catalytic applications, Surf. Coat. Technol. 123 (2000) 122–128, https://doi.org/10.1016/S0257-8972(99)00520-4.

[27] C. Agrafiotis, A. Tsetsekou, The effect of processing parameters on the properties of γ-alumina washcoats deposited on ceramic honeycombs, J. Mater. Sci. 35 (2000) 951–960, https://doi.org/10.1023/A:1004762827623.

[28] L. Giani, C. Cristiani, G. Groppi, E. Tronconi, Washcoating method for Pd/γ-Al_2O_3 deposition on metallic foams, Appl. Catal., B 62 (2006) 121–131, https://doi.org/10.1016/j.apcatb.2005.07.003.

[29] X. Yu, S.T. Tu, Z. Wang, Y. Qi, Development of a microchannel reactor concerning steam reforming of methanol, Chem. Eng. J. 116 (2006) 123–132, https://doi.org/10.1016/j.cej.2005.11.008.

[30] I. Cerri, M. Pavese, G. Saracco, V. Specchia, Premixed metal fibre burners based on a Pd catalyst, Catal. Today 83 (2003) 19–31, https://doi.org/10.1016/S0920-5861(03)00213-X.

[31] S.J. Lee, A. Gavriilidis, Au catalysts supported on anodised aluminium for low-temperature CO oxidation, Catal. Commun. 3 (2002) 425–428, https://doi.org/10.1016/S1566-7367(02)00161-9.

[32] J. Ganley, K. Riechmann, E. Seebauer, R. Masel, Porous anodic alumina optimized as a catalyst support for microreactors, J. Catal. 227 (2004) 26–32, https://doi.org/10.1016/j.jcat.2004.06.016.

[33] M. Valentini, G. Groppi, C. Cristiani, M. Levi, E. Tronconi, P. Forzatti, The deposition of γ-Al_2O_3 layers on ceramic and metallic supports for the preparation of structured catalysts, Catal. Today 69 (2001) 307–314, https://doi.org/10.1016/S0920-5861(01)00383-2.

[34] J.P. Reymond, Structured supports for noble catalytic metals: stainless steel fabrics and foils, and carbon fabrics, Catal. Today 69 (2001) 343–349, https://doi.org/10.1016/S0920-5861(01)00388-1.

[35] R. Zapf, G. Kolb, H. Pennemann, V. Hessel, Basic study of adhesion of several alumina-based washcoats deposited on stainless steel microchannels, Chem. Eng. Technol. 29 (2006) 1509–1512, https://doi.org/10.1002/ceat.200600204.

[36] V. Sebastián, O. de la Iglesia, R. Mallada, L. Casado, G. Kolb, V. Hessel, J. Santamaría, Preparation of zeolite films as catalytic coatings on microreactor channels, Microporous Mesoporous Mater. 115 (2008) 147–155, https://doi.org/10.1016/j.ces.2007.02.034.

[37] G. Germani, A. Stefanescu, Y. Schuurman, A.C. van Veen, Preparation and characterization of porous alumina-based catalyst coatings in microchannels, Chem. Eng. Sci. 62 (2007) 5084–5091, https://doi.org/10.1016/j.ces.2007.02.034.

[38] Y.S. Lin, K.J. de Vries, A.J. Burggraaf, Thermal stability and its improvement of the alumina membrane top-layers prepared by sol-gel methods, J. Mater. Sci. 26 (1991) 715–720, https://doi.org/10.1007/BF00588309.

[39] C. Agrafiotis, A. Tsetsekou, The effect of powder characteristics on washcoat quality. Part I: alumina washcoats, J. Eur. Ceram. Soc. 20 (2000) 815–824, https://doi.org/10.1016/S0955-2219(99)00218-6.

[40] V.T. Zaspalis, W. Van Praag, K. Keizer, J.R.H. Ross, A.J. Burggraaf, Synthesis and characterization of primary alumina, titania and binary membranes, J. Mater. Sci. 27 (1992) 1023–1035, https://doi.org/10.1007/BF01197657.

[41] K. Birdi, Handbook of Surface and Colloid Chemistry, second ed., CRC Press, Boca Raton, 2002.

[42] P. Jiang, G. Lu, Y. Guo, Y. Guo, S. Zhang, X. Wang, Preparation and properties of a γ-Al_2O_3 washcoat deposited on a ceramic honeycomb, Surf. Coat. Technol. 190 (2005) 314–320, https://doi.org/10.1016/j.surfcoat.2004.05.029.

[43] P.A.R. Cebollada, E. Garcia Bordejé, Optimisation of physical properties of γ-alumina coating microreactors used for the growth of a carbon nanofiber layer, Chem. Eng. J. 149 (2009) 447–454, https://doi.org/10.1016/j.cej.2009.02.016.

[44] X. Ying, L. Zhang, H. Xu, Y.L. Ren, Q. Luo, H.W. Zhu, H. Qu, J. Xuan, Efficient Fischer-Tropsch microreactor with innovative aluminizing pretreatment on stainless steel substrate for Co/Al_2O_3 catalyst coating, Fuel Process. Technol. 143 (2016) 51–59, https://doi.org/10.1016/j.fuproc.2015.11.005.

[45] Z.D. Xiang, P.K. Datta, Pack aluminisation of low alloy steels at temperatures below 700 °C, Surf. Coat. Technol. 184 (2004) 108–115, https://doi.org/10.1016/j.surfcoat.2003.10.046.

[46] J. Chen, H. Arandiyan, X. Gao, J. Li, Recent advances in catalysts for methane combustion, Catal. Surv. Asia 19 (2015) 140–171, https://doi.org/10.1007/s10563-015-9191-5.

[47] S.B.T.V. Choudhary, V.R. Choudhary, Catalysts for combustion of methane and lower alkanes review, Appl. Catal. A 234 (2002) 1–23, https://doi.org/10.1016/S0926-860X(02)00231-4.

[48] R. Burch, P.K. Loader, Investigation of Pt/Al_2O_3 and Pd/Al_2O_3 catalysts for the combustion of methane at low concentrations, Appl. Catal., B 5 (1994) 149–164, https://doi.org/10.1016/0926-3373(94)00037-9.

[49] M. Bhagiyalakshmi, R. Anuradha, S.D. Park, T.S. Park, W.S. Cha, H.T. Jang, Effect of bimetallic Pt-Rh and trimetallic Pt-Pd-Rh catalysts for low temperature catalytic combustion of methane, Bull. Korean Chem. Soc. 31 (2010) 120–124, https://doi.org/10.5012/bkcs.2010.31.01.120.

[50] N. Kinnunen, M. Suvanto, M. Moreno, A. Savimäki, K. Kallinen, T.-J. Kinnunen, T. Pakkanen, Methane oxidation on alumina supported palladium catalysts: effect of Pd precursor and solvent, Appl. Catal. A 370 (2009) 78–87, https://doi.org/10.1016/j.apcata.2009.09.018.

[51] J. Okal, M. Zawadzki, K. Baranowska, Methane combustion over bimetallic Ru-Re/γ-Al_2O_3 catalysts: effect of Re and pretreatments, Appl. Catal., B 194 (2016) 22–31, https://doi.org/10.1016/j.apcatb.2016.04.038.

[52] Y. Mahara, T. Tojo, K. Murata, J. Ohyama, A. Satsuma, Methane combustion over Pd/$CoAl_2O_4$/Al_2O_3 catalysts prepared by galvanic deposition, RSC Adv. 7 (2017) 34530–34537, https://doi.org/10.1039/c7ra06150a.

[53] Q. Dong, S. Zhang, Z. Duan, Q. Zhou, An energy analysis of the catalytic combustion burner, Heat. Technol. Energy Eff. (2006) http://hdl.handle.net/1969.1/5530.

[54] D. Xiaochun, Applied studies on methane catalytic combustion development of a natural gas premixed catalytic burner and boiler for household applications. 2005; Sichuan University. Thesis in Chinese.

[55] C.M. Miesse, R.I. Masel, C.D. Jensen, M.A. Shannon, M. Short, Submillimeter-scale combustion, AlChE J. 50 (2004) 3206–3214, https://doi.org/10.1002/aic.10271.

[56] L. Olsson, B. Westerberg, H. Persson, E. Fridell, M. Skoglundh, B. Andersson, A kinetic study of oxygen adsorption/desorption and NO oxidation over Pt/Al_2O_3 catalysts, J. Phys. Chem. B 103 (1999) 10433–10439, https://doi.org/10.1021/jp9918757.

[57] M. O'Connell, G. Kolb, R. Zapf, Y. Men, V. Hessel, Bimetallic catalysts for the catalytic combustion of methane using microreactor technology, Catal. Today 144 (2009) 306–311, https://doi.org/10.1016/j.cattod.2008.10.053.

[58] H. Mei, C. Li, S. Ji, H. Liu, Modeling of a metal monolith catalytic reactor for methane steam reforming-combustion coupling, Chem. Eng. Sci. 62 (2007) 4294–4303, https://doi.org/10.1016/j.ces.2007.05.011.

[59] M. Mundhwa, C.P. Thurgood, Numerical study of methane steam reforming and methane combustion over the segmented and continuously coated layers of catalysts in a plate reactor, Fuel Process. Technol. 158 (2017) 57–72, https://doi.org/10.1016/j.fuproc.2016.12.002.

[60] M. Mundhwa, R.D. Parmar, C.P. Thurgood, A comparative parametric study of a catalytic plate methane reformer coated with segmented and continuous layers of combustion catalyst for hydrogen production, J. Power Sources 344 (2017) 85–102, https://doi.org/10.1016/j.jpowsour.2017.01.082.

[61] P. Zhou, D. Tarlet, Y. Fan, X. Hu, L. Luo, Water-in-oil emulsification in a bifurcated tree-like network: flow distribution properties and their impact on the emulsion polydispersity, Chem. Eng. Res. Des. 134 (2018) 420–433, https://doi.org/10.1016/j.cherd.2018.04.031.

[62] P. Zhou, D. Tarlet, M. Wei, Y. Fan, L. Luo, Novel multi-scale parallel mini-channel contactor for monodisperse water-in-oil emulsification, Chem. Eng. Res. Des. 121 (2017) 233–244, https://doi.org/10.1016/j.cherd.2017.03.010.

[63] V. Meille, S. Pallier, G. Santacruzbustamante, M. Roumanie, J. Reymond, Deposition of γ-Al_2O_3 layers on structured supports for the design of new catalytic reactors, Appl. Catal. A 286 (2005) 232–238, https://doi.org/10.1016/j.apcata.2005.03.028.

[64] Christopher John Bennett, John P. Coll, D.E. Debnath, Andrea Hawkins, W. Manning, Method of applying washcoat to monolithic substrate, United States Patent, US9144796B1, Sep. 29, 2015.

[65] E.B. Andrew, J.G. Stephen, J.L. Mark, Adhesion and coating integrity of washcoats and overcoats, Unite State Patent, US20100081563A1, Apr. 1, 2010.

[66] O. Ohara, Adhesives comprising polyvinyl alcohol bearing or mixed with substances bearing carboxyl groups, and a stabilizer, United States Patent. 1968.

[67] M. Wiśniewska, S. Chibowski, T. Urban, D. Sternik, Investigation of the alumina properties with adsorbed polyvinyl alcohol, J. Therm. Anal. Calorim. 103 (2011) 329–337, https://doi.org/10.1007/s10973-010-1040-1.

[68] C.C. Huang, Y.J. Huang, H.S. Wang, F.G. Tseng, Y.C. Su, A well-dispersed catalyst on porous silicon micro-reformer for enhancing adhesion in the catalyst-coating process, Int. J. Hydrogen Energy 39 (2014) 7753–7764, https://doi.org/10.1016/j.ijhydene.2014.03.029.

[69] Z. Chen, C. Weinberger, M. Tiemann, D. Kuckling, Organic polymers as porogenic structure matrices for mesoporous alumina and magnesia, Processes 5 (2017) 70.

[70] S. Katheria, G. Deo, D. Kunzru, Washcoating of Ni/$MgAl_2O_4$ catalyst on FeCralloy monoliths for steam reforming of methane, Energy Fuels 31 (2017) 3143–3153, https://doi.org/10.1021/acs.energyfuels.6b03423.

[71] S.S. Kim, S.J. Lee, S.C. Hong, Effect of CeO_2 addition to Rh/Al_2O_3 catalyst on N_2O decomposition, Chem. Eng. J. 169 (2011) 173–179, https://doi.org/10.1016/j.cej.2011.03.001.

[72] H. Qin, R. Jian, J. Bai, J. Tang, Y. Zhou, B. Zhu, D. Zhao, Z. Ni, L. Wang, W. Liu, Q. Zhou, X. Li, Influence of molecular weight on structure and catalytic characteristics of ordered mesoporous carbon derived from lignin, ACS Omega 3 (2018) 1350–1356, https://doi.org/10.1021/acsomega.7b01870.

[73] B.V. Velamakanni, J.C. Chang, F.F. Lange, D.S. Pearson, New method for efficient colloidal particle packing via modulation of repulsive lubricating hydration forces, Langmuir 6 (1990) 1323–1325, https://doi.org/10.1021/la00097a023.

[74] B. Delmon, P.A. Jacobs, R. Maggi, J.A. Martens, G. Poncelet, Preparation of catalysts VII: proceedings of the 7th international symposium on scientific bases for the preparation of heterogeneous catalysts, Elsevier, Louvain-la-Neuve, Belgium, 1998.

[75] M.D. Franke, W.R. Ernst, A.S. Myerson, Kinetics of dissolution of alumina in acidic solution, AlChE J. 33 (1987) 267–273, https://doi.org/10.1002/aic.690330213.

[76] C. Cristiani, M. Valentini, M. Merazzi, S. Neglia, P. Forzatti, Effect of ageing time on chemical and rheological evolution in γ-Al_2O_3 slurries for dip-coating, Catal. Today 105 (2005) 492–498, https://doi.org/10.1016/j.cattod.2005.06.020.

[77] A.S. Rao, Effect of the surface active agents on the rheology of aqueous alumina slips, Ceram. Int. 14 (1988) 17–25, https://doi.org/10.1016/0272-8842(88)90013-2.

[78] J. Ayastuy, N. Gamboa, M. González-Marcos, M. Gutiérrez-Ortiz, CuO/CeO_2 washcoated ceramic monoliths for CO-PROX reaction, Chem. Eng. J. 171 (2011) 224–231, https://doi.org/10.1016/j.cej.2011.03.006.

[79] G. Landi, P.S. Barbato, A. Di Benedetto, L. Lisi, Optimization of the preparation method of CuO/CeO_2 structured catalytic monolith for CO preferential oxidation

in H_2-rich streams, Appl. Catal., B 181 (2016) 727–737, https://doi.org/10.1016/j.apcatb.2015.08.040.
[80] M.A. Kumar, K. Deepak, Effect of method of preparation on activity of Pd/Al_2O_3 monolith catalysts, Can. J. Chem. Eng. 88 (2010) 367–375, https://doi.org/10.1002/cjce.20288.
[81] J.M. Zamaro, M.A. Ulla, E.E. Miró, Zeolite washcoating onto cordierite honeycomb reactors for environmental applications, Chem. Eng. J. 106 (2005) 25–33, https://doi.org/10.1016/j.cej.2004.11.003.
[82] M. Brishti, K. Deepak, Washcoating of different zeolites on cordierite monoliths, J. Am. Ceram. Soc. 91 (2008) 64–70, https://doi.org/10.1111/j.1551-2916.2007.02032.x.
[83] S. Zhao, J. Zhang, D. Weng, X. Wu, A method to form well-adhered γ-Al_2O_3 layers on FeCrAl metallic supports, Surf. Coat. Technol. 167 (2003) 97–105, https://doi.org/10.1016/S0257-8972(02)00859-9.
[84] O. Deutschmann, R. Schmidt, F. Behrendt, J. Warnat, Numerical modeling of catalytic ignition, Symposium (International) on Combustion. 26 (1996) 1747–1754. doi: 10.1016/S0082-0784(96)80400-0.
[85] S. Oh, P. Mitchell, R. Siewert, Methane oxidation over noble metal catalysts as related to controlling natural gas vehicle exhaust emissions, Catalytic control of air pollution. ACS Publication, Washington, DC, 1992.
[86] V.A. Drozdov, P.G. Tsyrulnikov, V.V. Popovskii, N.N. Bulgakov, E.M. Moroz, T.G. Galeev, Comparative study of the activity of Al-Pd and Al-Pt catalysts in deep oxidation of hydrocarbons, React. Kinet. Catal. Lett. 27 (1985) 425–427, https://doi.org/10.1007/bf02070487.
[87] L. Ma, D.L. Trimm, C. Jiang, The design and testing of an autothermal reactor for the conversion of light hydrocarbons to hydrogen I. The kinetics of the catalytic oxidation of light hydrocarbons, Appl. Catal. A 138 (1996) 275–283, https://doi.org/10.1016/0926-860X(95)00301-0.
[88] H. Arai, T. Yamada, K. Eguchi, T. Seiyama, Catalytic combustion of methane over various perovskite-type oxides, Appl. Catal., A 26 (1986) 265–276, https://doi.org/10.1016/S0166-9834(00)82556-7.
[89] P. Barbato, G. Landi, R. Pirone, G. Russo, A. Scarpa, Auto-thermal combustion of CH_4 and CH_4-H_2 mixtures over bi-functional Pt-$LaMnO_3$ catalytic honeycomb, Catal. Today 147 (2009) S271–S278, https://doi.org/10.1016/j.cattod.2009.07.018.
[90] P.S. Barbato, A. Di Benedetto, V. Di Sarli, G. Landi, R. Pirone, High-pressure methane combustion over a perovskyte catalyst, Ind. Eng. Chem. Res. 51 (2011) 7547–7558, https://doi.org/10.1021/ie201736p.
[91] D.G. Norton, D.G. Vlachos, Combustion characteristics and flame stability at the microscale: a CFD study of premixed methane/air mixtures, Chem. Eng. Sci. 58 (2003) 4871–4882, https://doi.org/10.1016/j.ces.2002.12.005.
[92] D. Neumann, G. Veser, Catalytic partial oxidation of methane in a high-temperature reverse-flow reactor, AlChE J. 51 (2005) 210–223, https://doi.org/10.1002/aic.10284.
[93] M. Reinke, J. Mantzaras, R. Bombach, S. Schenker, A. Inauen, Gas phase chemistry in catalytic combustion of methane/air mixtures over platinum at pressures of 1 to 16 bar, Combust. Flame 141 (2005) 448–468, https://doi.org/10.1016/j.combustflame.2005.01.016.
[94] A. Di Benedetto, G. Landi, V. Di Sarli, P.S. Barbato, R. Pirone, G. Russo, Methane catalytic combustion under pressure, Catal. Today 197 (2012) 206–213, https://doi.org/10.1016/j.cattod.2012.08.032.
[95] M. Reinke, J. Mantzaras, R. Schaeren, R. Bombach, A. Inauen, S. Schenker, High-pressure catalytic combustion of methane over platinum: in situ experiments and detailed numerical predictions, Combust. Flame 136 (2004) 217–240, https://doi.org/10.1016/j.combustflame.2003.10.003.
[96] S.R. Vaillant, A.S. Gastec, Catalytic combustion in a domestic natural gas burner, Catal. Today 47 (1999) 415–420, https://doi.org/10.1016/S0920-5861(98)00324-1.
[97] K. Narui, H. Yata, K. Furuta, A. Nishida, Y. Kohtoku, T. Matsuzaki, Effects of addition of Pt to PdO/Al_2O_3 catalyst on catalytic activity for methane combustion and TEM observations of supported particles, Appl. Catal. A 179 (1999) 165–173, https://doi.org/10.1016/S0926-860X(98)00306-8.
[98] K. Murata, Y. Mahara, J. Ohyama, Y. Yamamoto, S. Arai, A. Satsuma, The metal-support interaction concerning the particle size effect of Pd/Al_2O_3 on methane combustion, Angew. Chem. Int. Ed. 56 (2017) 15993–15997, https://doi.org/10.1002/anie.201709124.
[99] C. Bozo, N. Guilhaume, E. Garbowski, M. Primet, Combustion of methane on CeO_2–ZrO_2 based catalysts, Catal. Today 59 (2000) 33–45, https://doi.org/10.1016/S0920-5861(00)00270-4.
[100] Y. Ozawa, Y. Tochihara, A. Watanabe, M. Nagai, S. Omi, Deactivation of Pt·PdO/Al_2O_3 in catalytic combustion of methane, Appl. Catal. A 259 (2004) 1–7, https://doi.org/10.1016/j.apcata.2003.09.029.
[101] J.H. Lee, D.L. Trimm, Catalytic combustion of methane, Fuel Process. Technol. 42 (1995) 339–359, https://doi.org/10.1016/0378-3820(94)00091-7.
[102] W.R. Schwartz, D. Ciuparu, L.D. Pfefferle, Combustion of methane over palladium-based catalysts: catalytic deactivation and role of the support, J. Phys. Chem. C 116 (2012) 8587–8593, https://doi.org/10.1021/jp212236e.